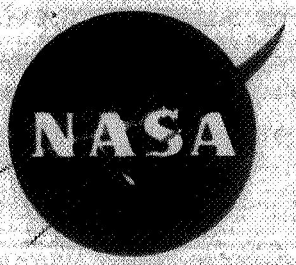

NASA CR-72812

FINAL REPORT

INVESTIGATION TO DEVELOP A DIRECT MELT FIBERIZATION PROCESS FOR PRODUCTION OF OXIDE FIBERS

by

M. Basche and R. D. Veltri

Prepared for

NATIONAL AERONAUTICS AND SPACE ADMINISTRATION

LEWIS RESEARCH CENTER

OCTOBER 30, 1970

CONTRACT NO. NAS3-13212
A. ANGLIN PROJECT MANAGER
NASA LEWIS RESEACH CENTER
CLEVELAND, OHIO

United Aircraft Research Laboratories

UNITED AIRCRAFT CORPORATION

EAST HARTFORD, CONNECTICUT

FINAL REPORT

INVESTIGATION TO DEVELOP A DIRECT MELT FIBERIZATION PROCESS FOR PRODUCTION OF OXIDE FIBERS

by

M. Basche and R. D. Veltri

UNITED AIRCRAFT RESEARCH LABORATORIES

East Hartford, Connecticut 06108

Prepared for

NATIONAL AERONAUTICS AND SPACE ADMINISTRATION

Lewis Research Center

October 30, 1970

CONTRACT NAS3-13212

NASA Lewis Research Center
Cleveland, Ohio
A. Anglin, Project Manager

TABLE OF CONTENTS

LIST OF ILLUSTRATIONS

LIST OF ILLUSTRATIONS (Cont'd)

ABSTRACT

The production of aluminum oxide fibers by a direct melt fiberization process was studied. Molybdenum proved to be a satisfactory material for holding molten aluminum-oxide for short periods of time and a successful crucible and orifice design was developed. Although the program was primarily experimental, a short computer program was run to aid in defining the state of fluid flow through the crucible orifice. The experimental results and the calculations both led to the conclusion that the molten liquid flow through the squirting orifice was laminar in nature and the break-up of the liquid aluminum oxide jet was caused by surface tension forces (i.e. free jet dynamics) and not by turbulence produced within the jet orifice.

Only short fibers of aluminum oxide were obtained under this program due to the aforementioned jet break-up. Attempts to stabilize the stream by cooling or deposition of a solid on the surface of the liquid jet were unsuccessful. The stabilization studies were, however, inconclusive in that optimum positioning of the stabilization and cooling media was not attained due to equipment limitations found later in the program.

SUMMARY

Under the program herein described, the production of aluminum oxide fibers by a direct melt fiberization process was studied. Molybdenum proved to be a satisfactory material for holding molten aluminum-oxide for short periods of time and a successful crucible and orifice design was developed. Although the program was primarily experimental, a short computer program was run to aid in defining the state of fluid flow through the crucible orifice. The experimental results and the calculations both led to the conclusion that the molten liquid flow through the squirting orifice was laminar in nature and the break-up of the liquid aluminum-oxide jet was caused by surface tension forces (i.e. free jet dynamics) and not by turbulence produced within the jet orifice.

Only short fibers of aluminum oxide were obtained under this program due to the aforementioned jet break-up. Attempts to stabilize the stream by cooling or deposition of a solid on the surface of the liquid jet were unsuccessful. The stabilization studies were, however, inconclusive in that optimum positioning of the stabilization and cooling media was not attained due to equipment limitations found later in the program.

INTRODUCTION

For the past several years, intensive research has been in progress in a search for new and improved filamentary materials for use as structural reinforcements. Filaments of boron, boron compounds, silicon carbide, and aluminum oxide have shown considerable promise for this application, and research in this area has turned to the development of manufacturing processes which will allow the economical production of such filaments at high rates. One such process is the continuous solidification of a free jet of molten material.

METHOD OF APPROACH

One approach to the production of continuous aluminum oxide filaments directly from a melt involves the formation of a stable, free jet of aluminum oxide and the extraction of heat from the jet at a rate sufficient to produce a continuously solidifying filament. However, a free liquid jet tends to break up into droplets at some distance from the orifice. Droplet formation is caused by the high interfacial tension between the liquid in the jet and the surrounding atmosphere and is preceded by the development of a capillary wave on the surface of the jet, the amplitude of which grown with time. In order to form a filament, the heat transfer rate must be sufficient to solidify the filament before the wave amplitude reaches some critical value. This may be accomplished either by increasing the rate of heat transfer or by reducing the rate of increase of the wave amplitude for a fixed cooling rate by stabilizing the jet.

Research conducted to date has not turned up any metal or metallic oxide which can be fiberized by free fall in an inert, quiescent gas. It was thus apparent that cooling or cooling together with stabilization might have to be

employed in order to produce aluminum oxide fiber from the melt. The necessary cooling was to be applied by means of a flow of gas transverse to the axis of the molten jet since the transverse flow pattern has been found to be the only one which does not excite either the capillary or sinous modes of instability.

If stabilization of the liquid jet was necessary, it was to be accomplished by depositing a solid coherent film on the surface of the jet; a carbon film, for example, could be deposited on the surface of the liquid jet. The stabilizing effect of a surface film is responsible for the successful formation of fibers of tin, lead, and aluminum by a direct melt process.

Dimensional Analysis of the Process

A qualitative mathematical analysis of the direct melt fiber process may be performed by utilizing some of the results of the theory of capillary instability. It has been verified, both theoretically and experimentally (Refs. 1,2,3) that the time required for the disintegration of a liquid jet is given by:

$$t_i = A \left[\frac{\sqrt{d^3 \rho}}{8T} + \frac{3 \mu d}{\alpha T} \right] \qquad (1)$$

The symbols have the following meanings:

d - jet diameter, cm

ρ - mass density of molten metal, gm/cm^3

T - surface tension, dyne/cm

μ - viscosity, dyne sec/cm^2

A jet of nonviscous fluid has a disintegration time proportional to the 1.5 power of jet diameter while a viscous fluid (such as glass) has a disintegration time proportional to the first power of jet diameter. The dependence of these two limiting cases on surface tension and density is also quite

different, as may be seen by an inspection of Eq. (1). Since we were only interested in a qualitative analysis, we were not concerned with the actual values of the constants A and α. We may, in fact, assign the value A = 1 by stretching the time scale.

The quantity of heat contained in a unit length of molten metal jet is

$$\frac{H_f \rho \pi d^2}{4}$$

The time required to extract this heat is therefore

$$t_H = \frac{H_f \rho d}{4h\theta} \tag{2}$$

where H_f = heat of fusion, cal/gm

h = heat transfer coefficient, cal/sec cm^2 °C

θ = melting temperature, °C

A dimensionless quantity governing the stability of a jet with heat transfer may be obtained by forming the ratio t_i/t_H:

$$\frac{t_i}{t_H} = \frac{\sqrt{2d}}{\rho T}\frac{h\theta}{H_f} + \frac{12\mu h\theta}{\alpha \rho T H_f} \tag{3}$$

This ratio governs the fiber formation process. It is obvious that fiber formation becomes easier for increasing values of t_i/t_H. An idea of the relative difficulty of fiber formation for different materials may be obtained by ignoring the viscosity term in Eq. (3) and evaluating the quantity

$$\frac{\theta}{H_f \sqrt{\rho T}} = \text{F.P.} = \text{Fiberization Potential}$$

which depends only on the physical properties of the material. The necessary data and subsequently calculated values of $\theta/H_f\sqrt{\rho T}$ for some materials are shown in Table 1.

Table 1

Fiberization Potential of Various Materials

Material	ρ, $\frac{gm}{cm^3}$	T, $\frac{dyne}{cm}$	H_f, $\frac{cal}{gm}$	θ, °C	$\frac{\theta}{H_f \sqrt{\rho T}}$
Al	2.70	840	94.5	660.1	.147
Au	19.3	790	16.1	1063	.053
Ag	10.49	800	25	960.5	.042
Cd	8.64	630	13.2	320.9	.329
Cu	8.96	1103	50.6	1083	.215
Pb	11.34	453	6.26	327.4	.730
Pt	21.45	1819	26.9	1769	.333
Zn	7.14	753	24.09	419.5	.237
Sn	7.3	526	14.0	231.9	.267
Fe	7.87	1706	7.89	1534	1.68
Cr	7.14	1590 $\pm$ 50	96	1875	.183
Ni	8.9	1630 $\pm$ 140	73.8	1453	.163
Be	1.85	1650 (est.)	260	1284	.089
Mn	7.43	880 (est.)	63.7	1245	.242
B	2.34	2500 (est.)	480	2050	.056
Al_2O_3	4.0	700	25.5	2050	1.52

(Data obtained from Refs. 4-7)

An examination of this data shows that the easiest materials to fiberize should be iron, lead and aluminum oxide.

Equation (3) does not give a complete description of this fiber process because the surface tension and viscosity are functions of the solid fraction contained in the solidifying filament, due to the action of cooling. A qualitative picture of the desired correction may be obtained by writing T and μ as functions of the heat ratio q/H_f, where q is the quantity of heat which has been extracted from the molten material per unit of jet length. When $q = 0$, the jet is entirely liquid and the jet is completely solid when $q = H_f$ $(q/H_f = 1)$. The heat extracted from the molten jet can also be expressed as

$$q = \pi d\, h\, \theta\, t \qquad (4)$$

where t is the length of time that cooling has been applied. Now, the surface tension and viscosity of a completely molten metal may be defined as T_o, μ_o,

respectively. As heat is extracted (at constant temperature), solid material appears in the melt and the surface tension and viscosity change. When the melt has completely solidified, the surface tension is effectively zero, and the viscosity infinite. It is appreciated that the latter statement is not strictly true in a physical sense but it should be realized that we are trying to assess the propensity of a liquid to undergo surface deformation under the action of forces which are of the order of magnitude of the surface tension and inertia forces of the completely molten metal. Under these circumstances, it is convenient to describe the immobility of a solid surface under the action of such forces by saying that the surface tension is zero and the viscosity infinite. A functional relation which expresses this statement in a qualitative way is given by

$$T = T_o \left(1 - \frac{q}{H_f}\right)$$

$$\mu = \frac{\mu_o}{\left(1 - \frac{q}{H_f}\right)} \tag{5}$$

Substituting Eq. (5) into Eq. (3) we find:

$$\frac{t_i}{t_H} = \frac{h\theta}{H_f} \left[\frac{\sqrt{2d}}{T_o} \frac{1}{\left(1 - \frac{q}{Hf}\right)^{1/2}} + \frac{12\,\mu_o}{\alpha \rho T_o} \frac{1}{\left(1 - \frac{q}{H_f}\right)^2} \right] \tag{6}$$

$$\left(0 \leq \frac{q}{H_f} \leq 1\right)$$

It can be seen that, as q/H_f increases, the time ratio t_i/t_H increases from a value t_i/t_H to infinity. Cooling, therefore, exerts a stabilizing effect on a liquid jet.

This analysis does not take into account the various schemes for stabilizing a jet by producing a surface coating, but it does give a clear picture of the physical behavior of a liquid jet with cooling.

Variables Affecting Filament Formation

In the previous mathematical analysis factors influencing stable jet length, the flow of molten fluid from the exit nozzle was assumed to be laminar. Transition to turbulent fluid flow, whether due to Reynold's number effects or local surface activated tripping of the stream, would yield such short jet lengths (Ref. 8) that formation of filaments would be extremely difficult. Factors in the design of the exit orifice to insure proper flow such as chamfer angle, depth of chamfer to prevent cavitation (Ref. 9) and a smooth entry flow transition regime (Ref. 10) were taken into account. A further number of practical considerations involved in the formation of such a jet will now be discussed.

Squirt Pressure - The stable length of a free jet has been found to be equal to the jet velocity multiplied by the disintegration time, t_i. An important factor affecting the length of stable jet which was not previously considered is the turbulence within the jet produced by flow through the orifice of the crucible. The net effect of turbulence is a reduction in the disintegration time (t_i) at high jet velocities. A typical curve illustrating this factor is shown in Fig. 1a for water (Ref. 11). The corresponding curve of t_i versus V is shown in Fig. 1b. It is obvious from an inspection of these figures that the squirting pressure should be chosen so as to give the maximum length of stable jet. The optimum squirting pressure was one of the variables investigated under this program.

Crucible Material Selection - Compatibility studies were conducted between aluminum oxide and several candidate crucible materials. Because of the high melting point of aluminum oxide only tungsten, molybdenum, tantalum, and iridium were considered to be suitable for this application. Molybdenum was chosen as the nozzle material. Tantalum, which has a high enough melting point (2996°C)

FIG. 1

EFFECT OF JET VELOCITY ON STABLE LENGTH

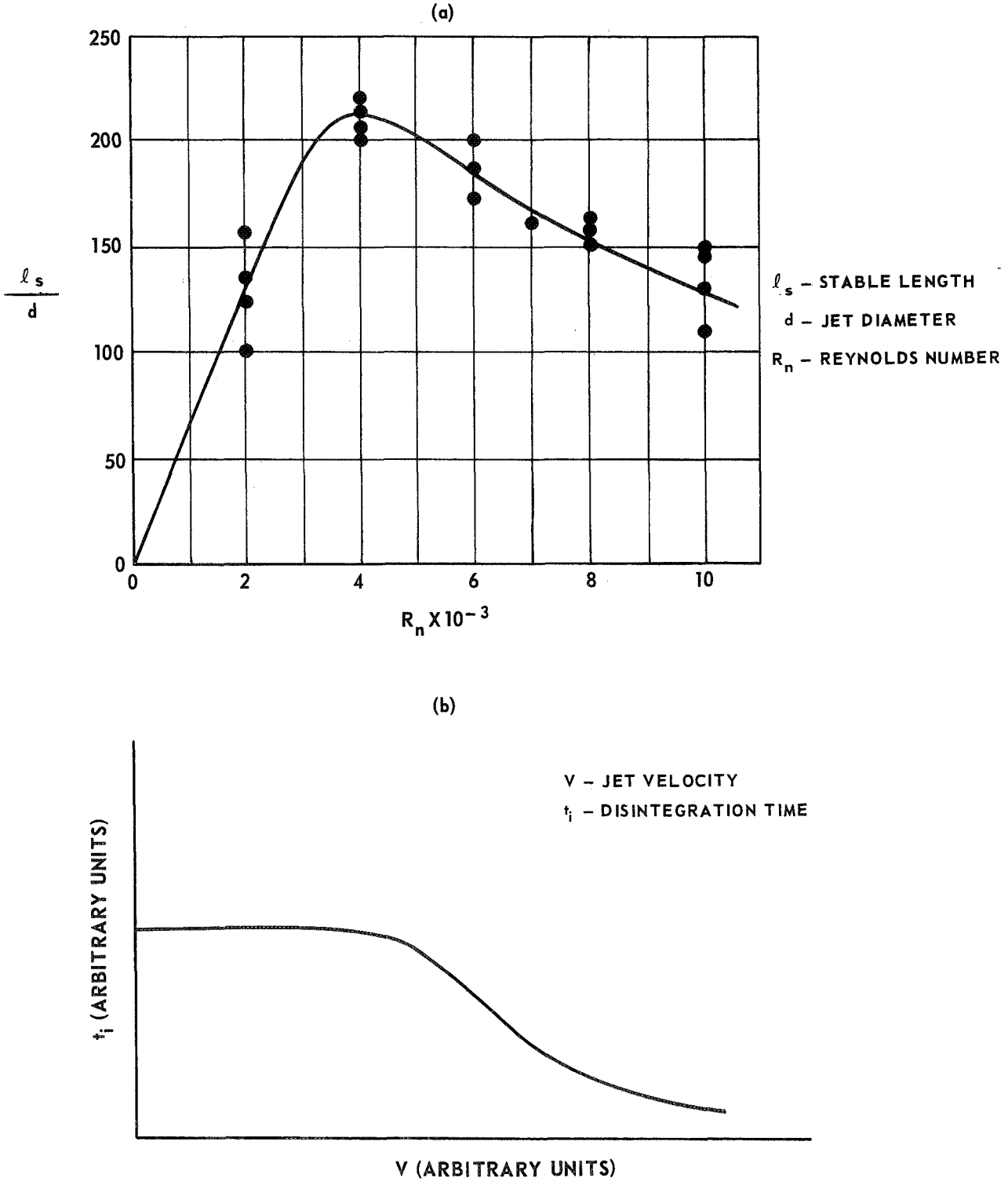

and is easily fabricated, underwent severe embrittlement and grain boundary attack when aluminum oxide was kept molten for even short periods of time. Tungsten (M.P. 3410°C), which is more difficult to fabricate, would contain the molten aluminum oxide without observable damage to the container walls but contaminated the melt with migration of metallic tungsten particles throughout the molten oxide in periods of less than five minutes. Molybdenum (M.P. 2610°C) satisfied the needs of both fabrication and inertness toward the molten oxide for times up to 45 minutes. A photomicrograph of a cross section through a closed end nozzle in which polycrystalline aluminum oxide was melted and then solidified is shown in Fig. 2. No diffusion of either specie is in evidence. Iridium (M.P. 2454°C), another possible container material, was not investigated due to its high cost and difficulty of fabrication.

Crucible Design - The initial crucibles used for direct melt aluminum oxide fiberization studies at UARL were simple flat-bottomed closed-end tubes with electron-beam drilled orifice holes. The most serious problems encountered with this type of crucible were freezing of the aluminum oxide on the outside bottom of the crucible with subsequent plugging of the orifice and jet turbulence caused by the roughness of the electron-beam drilled hole. After several modifications, a crucible design evolved as shown in Fig. 3. The nozzle was assembled from four simple and relatively inexpensive molybdenum parts. The hole was drilled in the orifice disc prior to electron-beam welding of the disc to the tube. This procedure greatly facilitated the drilling of a proper orifice and allowed the hole to be correctly shaped. The skirt on the bottom of the crucible acted as a susceptor to heat the orifice and prevented the premature freezing of the aluminum oxide stream. This basic crucible configuration was used (with various orifice plates) throughout the program.

FIG. 2

MOLYBDENUM-ALUMINUM OXIDE INTERFACE

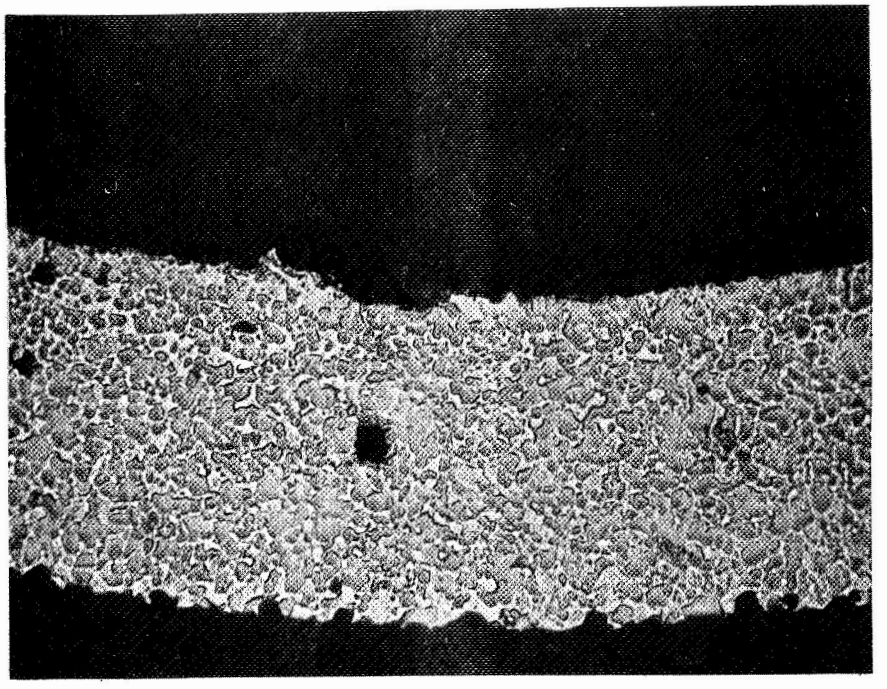

50X

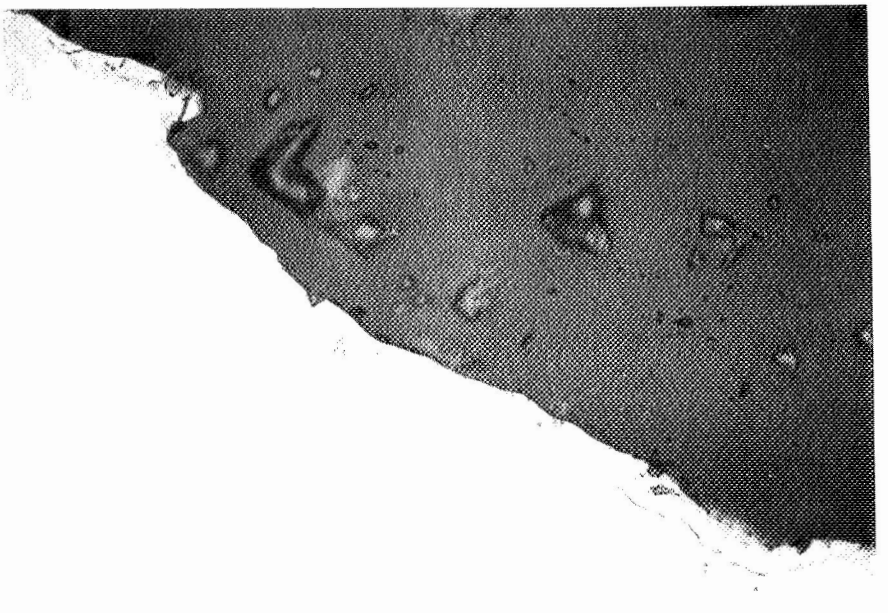

500X

FIG. 3

PRELIMINARY SQUIRTING NOZZLE ASSEMBLY

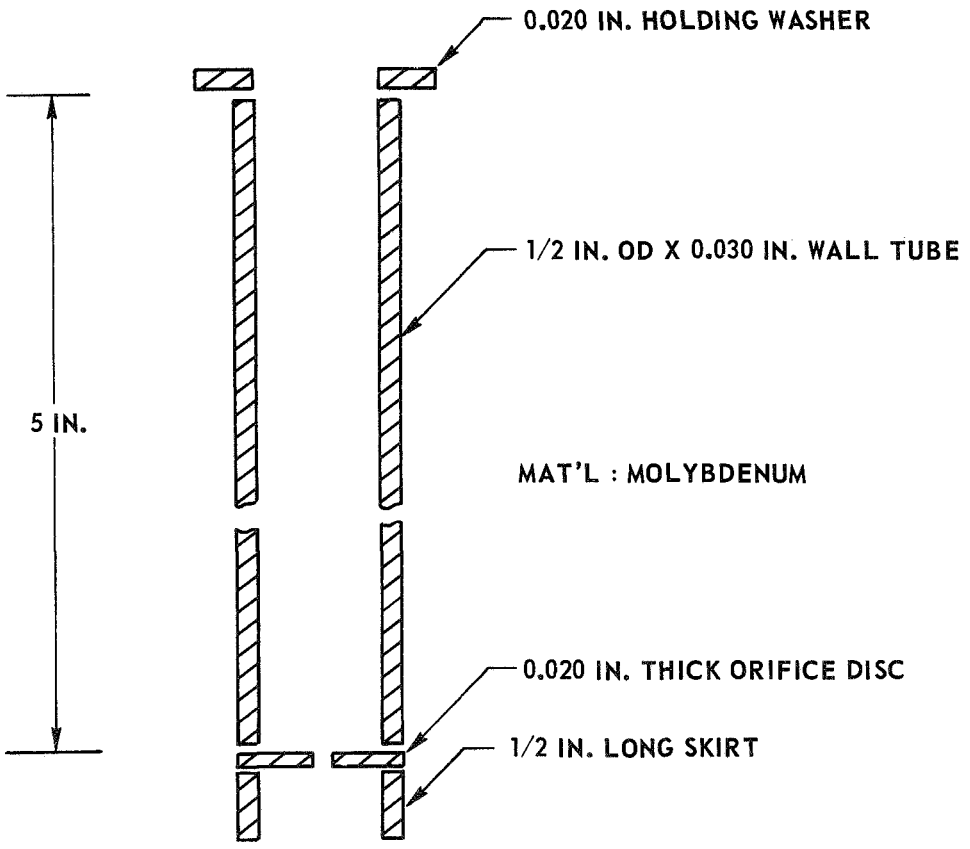

Crucible Orifice Design - The longitudinal profile of the orifice and the roughness of the walls of the orifice have a profound effect on the stability of the jet. It is well known that surface roughness induces turbulence and that such turbulence can be damped out by causing the orifice to taper in the direction of flow. For these reasons all orifice plates used in this investigation were of the general configuration as shown in Fig. 4. The precise orifice dimensions were considered to be one of the variables to be investigated under this program.

Melt Temperature - The temperature of the melt was one of the most critical variables in this process. If the melt was too hot (too much superheat), only "shot" would be formed when the squirt pressure was applied. On the other hand, if the melt temperature was too cold (very little superheat), it was almost impossible to get anything through the orifice of the crucible. The melt temperature, therefore, had to be accurately monitored and controlled in order to succeed with this process. A special heating control system was designed and assembled to provide control of the melt temperature to within 1°C of the set point and approximately 10°C absolute (the accuracy of the pyrometer).

Node Formation - Nodules are produced on melt-spun fiber when the fiber is bent to a sufficiently small radius to crack the solidified skin. Molten material then flows through the break at the same time that the skin reforms on the fresh surface.

Bending of the molten filament is caused largely by the axial velocity of the filament relative to that of the gaseous environment which results in flutter of the same kind observed when a flag waves in the breeze. The flutter amplitude increases with increasing filament velocity and decreasing filament density. The wavelength of this motion decreases with increasing velocity.

FIG. 4

NASA SPECIFIED ORIFICE

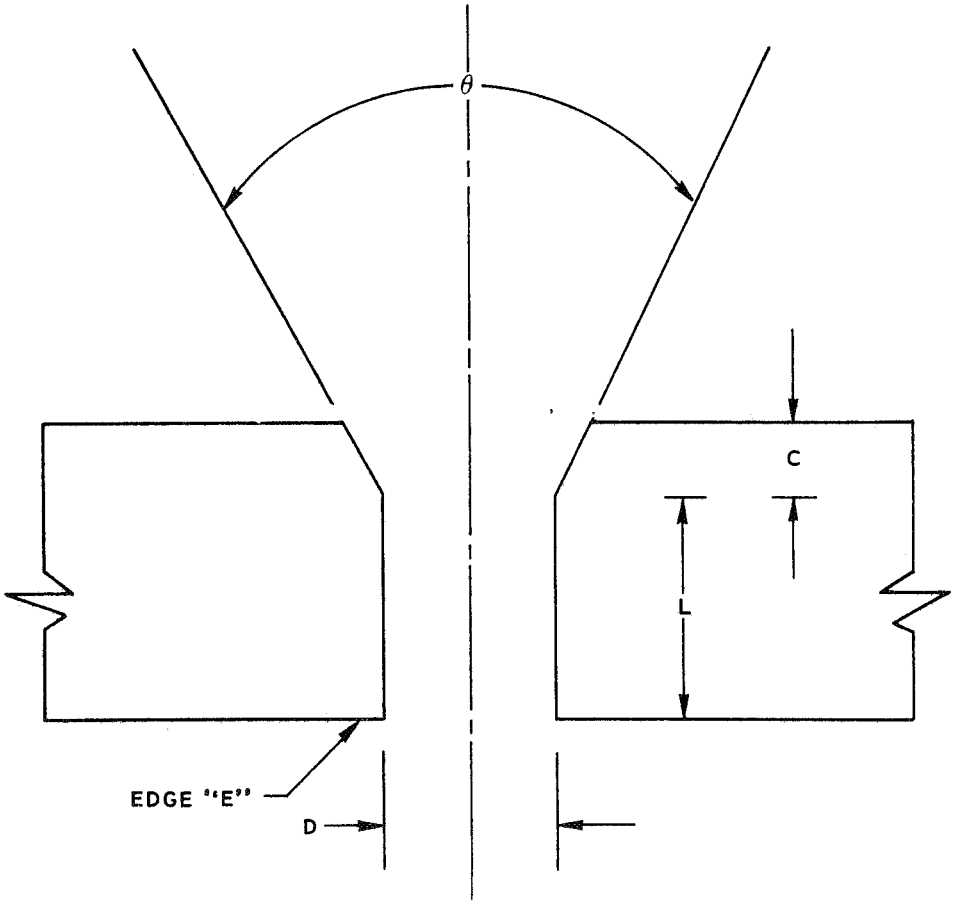

TYPE	D	C	L	θ
A	0.010 IN.	0.003 IN.	0.010 IN.	50°
B	0.008 IN.	0.002 IN.	0.016 IN.	50°
TOL.	± 0.001	± 0.001	± 0.001	±10°
EDGE "E" MUST BE SHARP				

A simple explanation of the mechanism which causes flutter can be found by considering the equilibrium of a length of filament being carried along by a gas stream. If the filament is oriented parallel to the gas velocity vector, a turning moment is produced which tends to rotate the filament to an orientation at right angles to the flow. The perpendicular position is stable; the parallel position is unstable. In a continuous filament, these aerodynamic forces are resisted by inertia and aerodynamic damping, resulting in a continuous wave motion.

No flutter should occur if the gas stream into which the filament is injected is flowing at the same velocity and in the same direction as the filament; however, the cooling rate is very low in this case. A gas flow at right angles to the filament should not cause flutter and also gives the best cooling rate. Therefore, it was planned that any cooling gas (air or helium + air) used to remove heat from the stream would be introduced perpendicularly to the molten jet.

Aluminum Oxide Alloy Systems - Aluminum oxide of high purity was the primary material used in this program. However, additions of other oxides to the aluminum oxide were made in order to study their effect on the fiberization process. The following binary oxide mixtures were approved for investigation under this program:

1. Complete Solid Solution - 70 percent Al_2O_3 - 30 percent CrO_2
   liquidus 2130°C - solidus 2075°C.
2. Eutectic Composition - 80 percent Al_2O_3 - 20 percent Y_2O_3
   melting point - 1860°C.
3. Wide Range Solidification - 80 percent Al_2O_3 - 20 percent SnO_2
   liquidus 1960°C - solidus 1620°C.
4. Eutectic Composition - 95 percent Al_2O_3 - 5 percent MgO
   melting point - 1950°C.

The effect of alloy addition on the molybdenum crucible compatibility was also studied.

EXPERIMENTAL PROCEDURES AND RESULTS

Melt Spin Apparatus

The apparatus that was used for preliminary experiments prior to the program is shown schematically in Fig. 5. This equipment was used to determine the accuracy of temperature control needed for the squirting process. It was soon evident that using the orifice plate as the temperature indicating target (as shown in Fig. 5) did not yield reproducible results; several runs made under the same conditions showed either no evidence of melting or resulted in oozing of the aluminum oxide through the orifice. In order to be able to squirt at a constant temperature, some form of automatic control was necessary that could maintain the aluminum oxide charge at any specific temperature during its entire molten stage. Since the change of viscosity with temperature for molten aluminum oxide was anticipated to be quite sharp, accurate temperature control was mandatory.

Temperature Control System - An automatic radiation ratio pyrometer was chosen as the sensing element for the temperature control system in order to minimize several of the errors normally associated with brightness pyrometer measurements.

To produce a linear increase in temperature with time, the output of the pyrometer was compared electronically to a ramp generated in the controller. The output of the comparator was then amplified and used to power a motor-driven potentiometer. The motor acted as an integrator thus yielding a low, steady-state error for the system. The potentiometer was used to set the triggering angle of a pair of silicon controlled rectifiers which, in turn, adjusted the input power to the saturable reactor that controlled the power output of the Lepel induction heater. The control system operated very well and maintained the crucible temperature to within approximately 10°C, (the accuracy of the

SCHEMATIC OF PRELIMINARY ALUMINA SQUIRTING APPARATUS

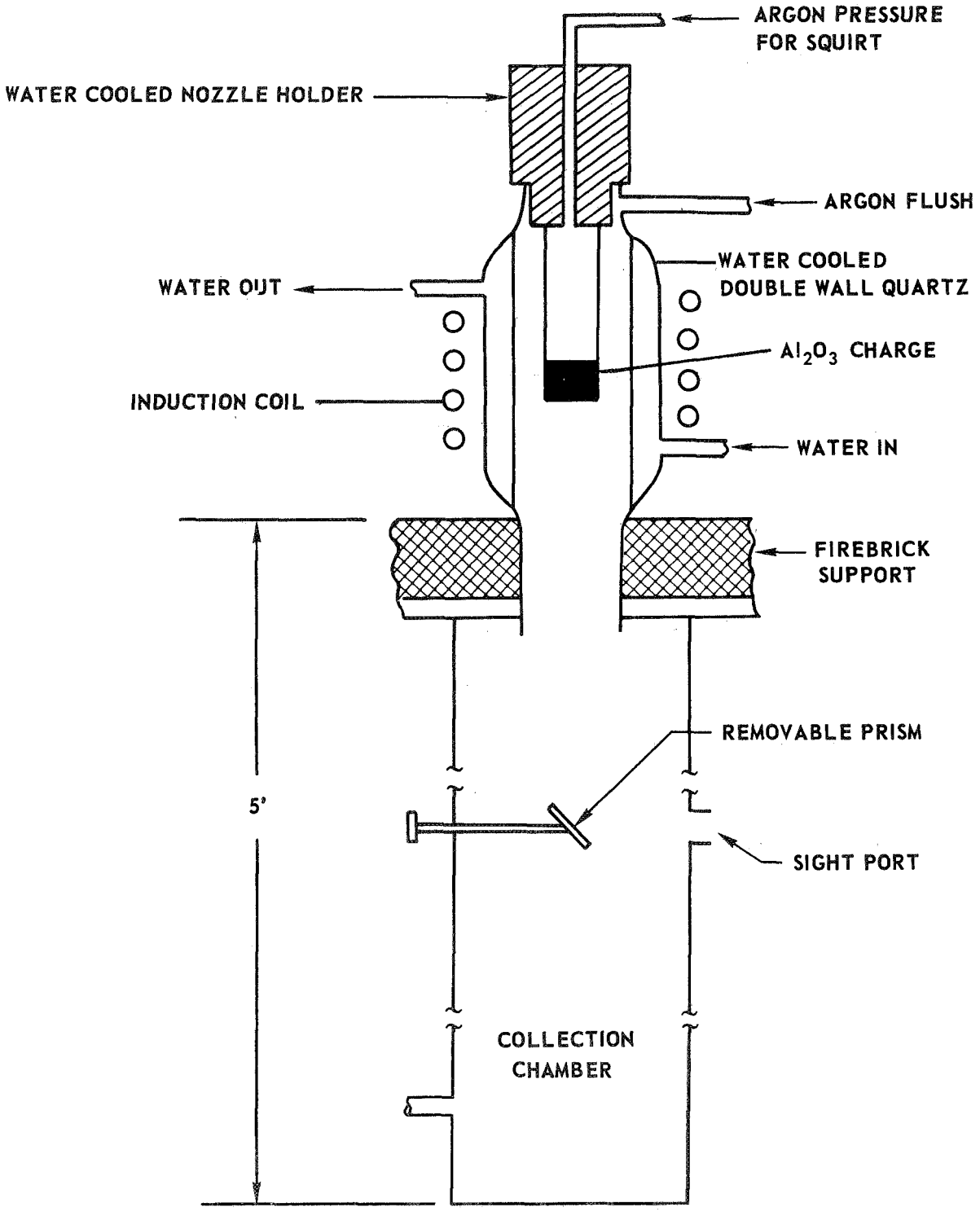

pyrometer). The major problem encountered with the controller was the thermal lag of the induction heating system which caused overshooting whenever the pyrometer came out of the automatic calibration cycle. This was simply eliminated by calibrating just prior to approaching final temperature and then locking-out the calibration cycle. The pyrometer was originally placed as shown in Figs. 6 and 7. The temperatures measured at this location were not uniform enough from run to run due to small differences in the coil or crucible location. To eliminate these problems a holding assembly was fabricated to position the two-color pyrometer directly above the squirting nozzle, where a quartz sight port allowed direct temperature measurement of the melt. A periscope was fabricated to provide observation of the melt through the pyrometer head. The entire assembly is shown in Fig. 8. The pyrometer was calibrated by observation of incipient melting of single crystal (sapphire) aluminum oxide within the nozzle. There were initial problems encountered with the pyrometer due to an instability in its output that caused sensing errors as high as 150°C. Replacement of the sensing unit eliminated all further problems with the temperature control system and the calibration experiments indicated the melting point of single crystal aluminum oxide to be 2055°C.

Nozzle Pressurization System - A gas pressurization system was assembled to provide low pressure purge gas to the crucible during melting and rapid pressure application when squirt conditions were reached. The system as originally assembled can be seen in Fig. 7. Precision gauges with overlapping ranges were used to monitor the gas pressure in the crucible. Both low pressure argon for purging and high pressure tank argon for squirting were controlled by the use of pressure regulators and flow meters as seen in the photograph shown in Fig. 6. The change from low pressure purge to high pressure squirt was controlled

COMPLETE MELT SPIN APPARATUS

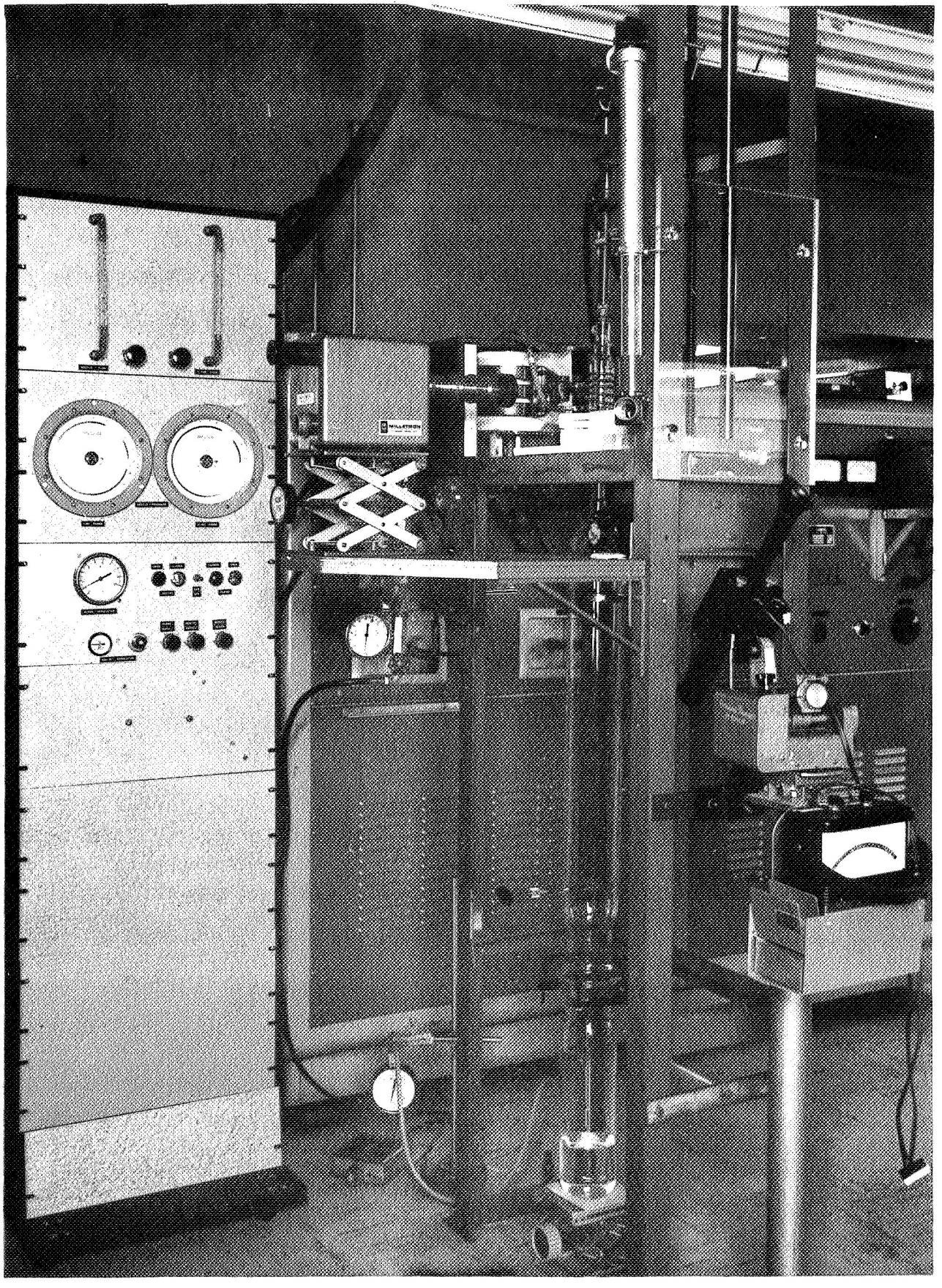

FIG. 7

MELT SPIN APPARATUS GAS CONTROL SYSTEM

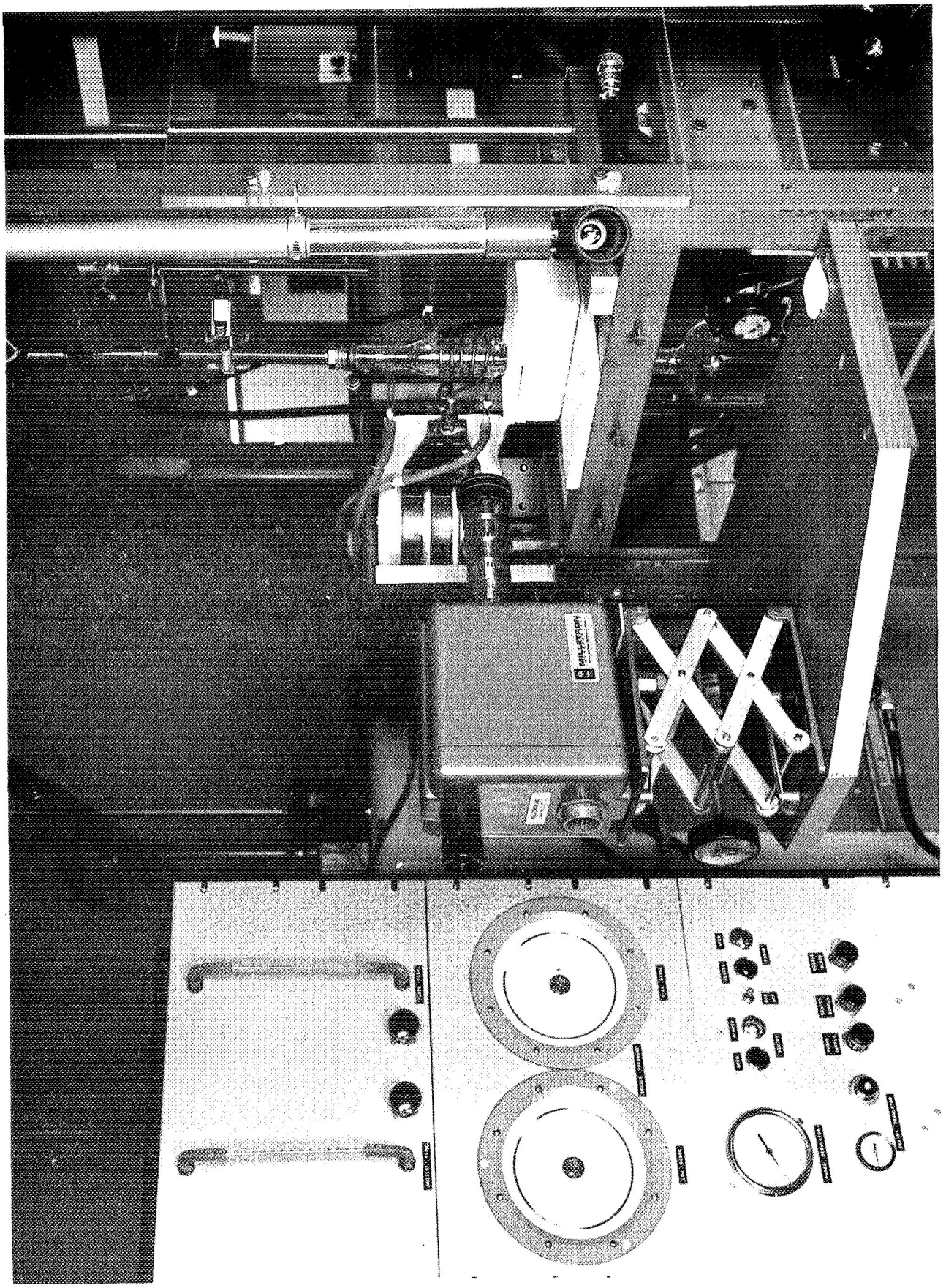

FIG. 8

ALUMINUM OXIDE MELT SPINNING APPARATUS

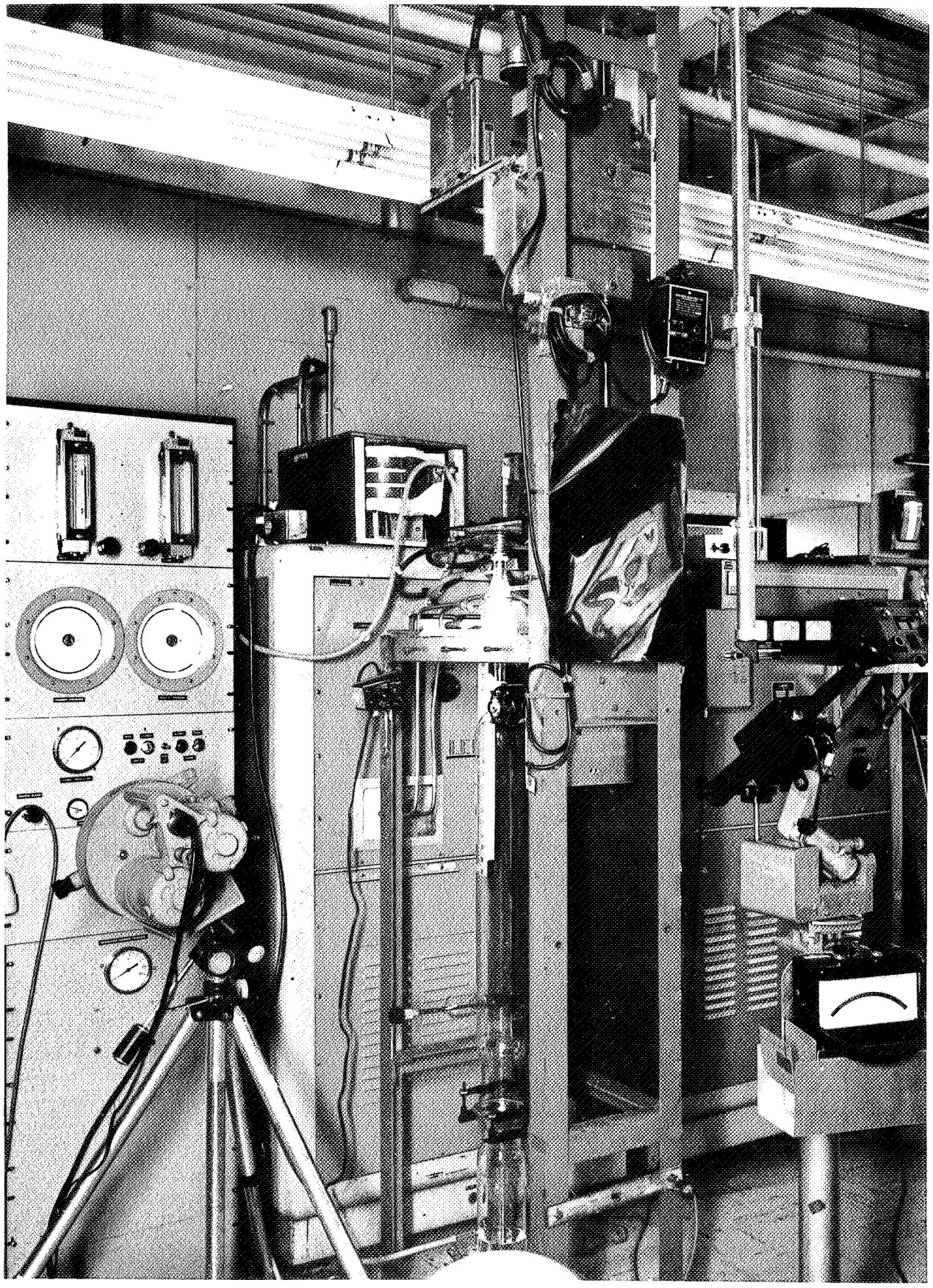

by solenoid valves. Originally the squirt pressures were relatively low (20 psi) and the flow meters shown in Fig. 7 were adequate; but as the squirt pressure was raised (50 psi) guarded high pressure flow meters as shown in Fig. 8 were necessary.

During the initial experiments, squirt pressure was applied when dripping or oozing of the melt was observed through the pyrometer monitoring the bottom of the orifice plate. This condition was unsatisfactory because wetting of the bottom plate prior to squirting would very often result in a plugged orifice. To eliminate this problem, the gas collection envelope was modified to support a 2 to 3 psia back pressure on the orifice plate. The pressure in the gas envelope was monitored by one of the precision pressure gauges (shown in Fig. 7) and controlled by means of a low pressure regulator. The release of chamber pressure when squirting conditions were reached was originally accomplished by the manual opening of a small hand valve. This system provided a relatively slow release of chamber pressure down to atmospheric which still allowed oozing of the molten alumina to take place. The apparatus was therefore modified to provide for fast release of chamber back-pressure by means of a solenoid valve. The system was rewired to actuate the release valve simultaneously with the application of squirt pressure. This last modification eliminated all further problems with oozing of the molten alumina.

Stream Velocity Measurements - A Fastax camera was set up to photograph the molten jet. A speed of 1000 frames per second was found to be sufficiently fast to provide clear photographs of the breakup of the stream. In order to accurately measure the stream velocity, a 100-cycle-per-second timing mark was automatically placed on the film during each run. A scale, lined up with the bottom of the crucible, provided the distance measurement for the velocity calculations. In

order to achieve good photographs of the molten jet at approximately 2000°C, several neutral density filters were needed on the camera. This necessitated using a separate illuminator for the distance scale. Figure 8 shows the Fastax camera, illuminator, and distance scale in position during a run and Fig. 9 is a time exposure taken during a squirting run. The many tracks seen in Fig. 9 are the tracers from individual droplets of aluminum oxide due to breakup of the stream under the particular conditions used for that experiment.

The movies taken of the squirting runs were also used to determine the length of the stable liquid jet before breakup into droplets.

Aluminum-Oxide Alloy Preparation - Aluminum oxide alloys with CrO_2 (30 percent), SnO_2 (20 percent), Y_2O_3 (20 percent), and MgO (5 percent) were prepared from carefully weighed and well-mixed, high-purity powders. Initial melts were made in the squirt apparatus using closed-end nozzles as the melting crucibles. This technique worked for the yttria and chromia alloys but was unsuccessful in the case of the SnO_2 alloy due to its decomposition and subsequent reaction with the crucible. High pressure melting equipment was not available and the SnO_2 alloy work was discontinued. Remelting in the closed-end nozzles of the CrO_2 and Y_2O_3 with additional material to provide large enough charges for squirting was performed, but this technique was abandoned because it did not yield a homogeneous mixture.

A series of arc melted buttons were then prepared from pressed oxide powders. Although a few squirt experiments were performed with these alloys this technique was also discarded due to lack of homogeneity in the buttons. In order to provide a large and uniform supply of the oxide alloys, new powder mixtures were prepared and melted in a large, high-temperature furnace. This technique was very successful in providing homogeneous alloys of aluminum oxide with yttria,

FIG. 9

TIME EXPOSURE OF MELT SPINNING EXPERIMENT

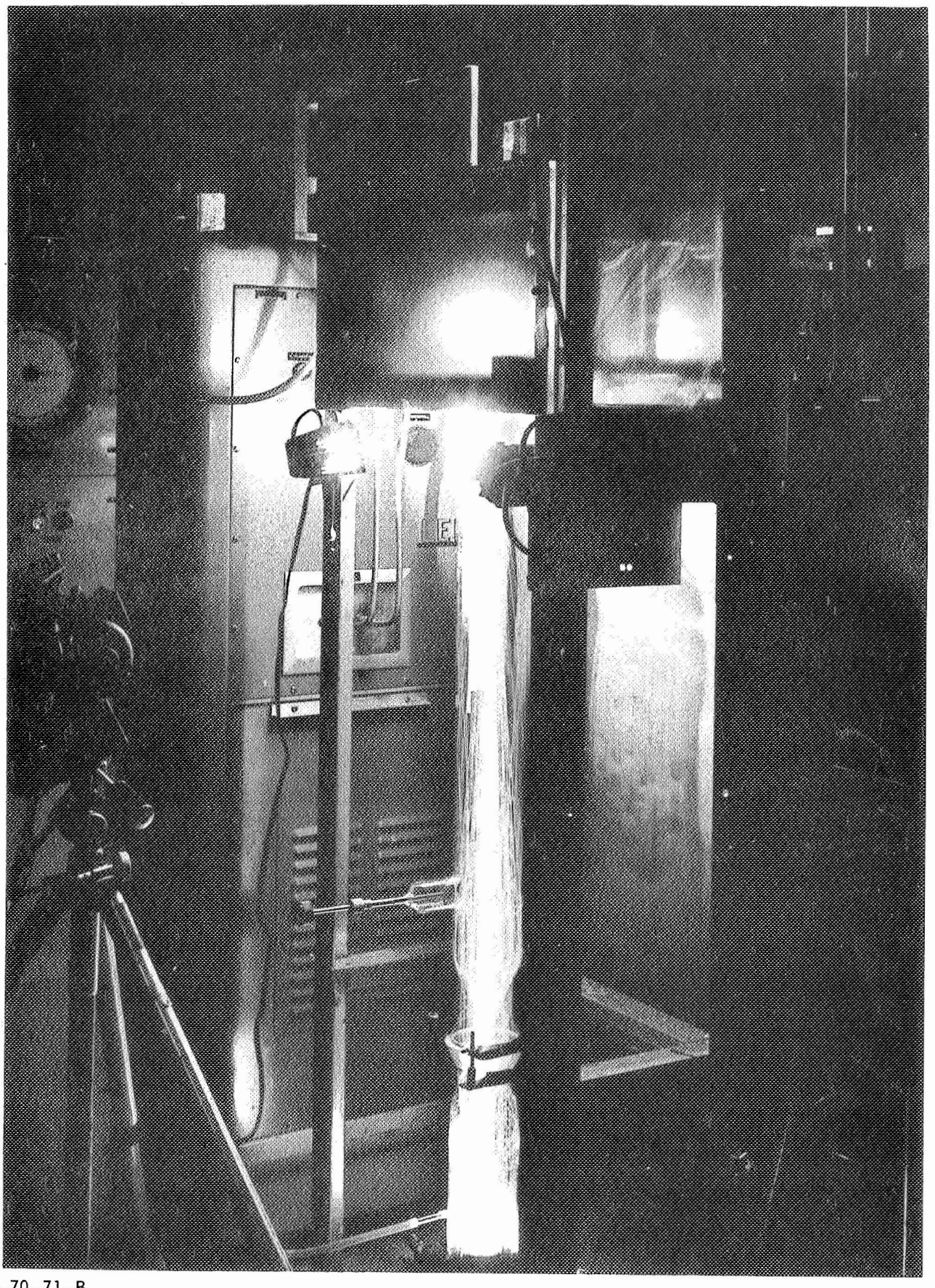

RL-70-71-B

chromia, and magnesia. Enough material was melted at one time for 12 squirting experiments of each alloy. X-ray and wet chemical analyses established that the charges were of the desired compositions.

Cooling and Jet Stabilization - When the stable jet length was increased to almost 3 inches, cooling and stabilization studies were initiated. Several water-cooled quartz heating assemblies were made incorporating various transverse flow coolers. A typical configuration is shown in Fig. 10. A cooling gas solenoid valve was wired into the gas control panel in such a manner as to permit operator control of the valve. In practice, the aluminum oxide stream was first started and then the cooling gas applied. This allowed direct observation and photography of the effects of the transverse flow on the stream. The transverse cooling gas (helium) did not introduce any lateral motion or periodic instability to the molten stream. It was felt, however, that for the cooling gas to be most effective, the apparatus used for these experiments needed major changes in order to get the cooling gas introduced directly below the exit orifice. Because of its relatively low position (2 1/2 inches below the orifice), the cooling was not effective in increasing the fiber lengths obtained with this equipment. There was not sufficient time remaining in the program to make the necessary changes in the heating assembly to place the transverse cooler at its optimum position.

Stabilization of the stream was attempted using methane and ammonia as stabilizing gases to produce solid carbon or aluminum nitride, respectively on the surface of the molten jet. The stabilization gas was introduced into both the outer flush and the transverse cooling manifold. However, since the collection envelope on the system was glass, the stabilization gas was limited to approximately 10 percent by volume of the total gas flow.

FIG. 10

TYPICAL EXPERIMENTAL APPARATUS

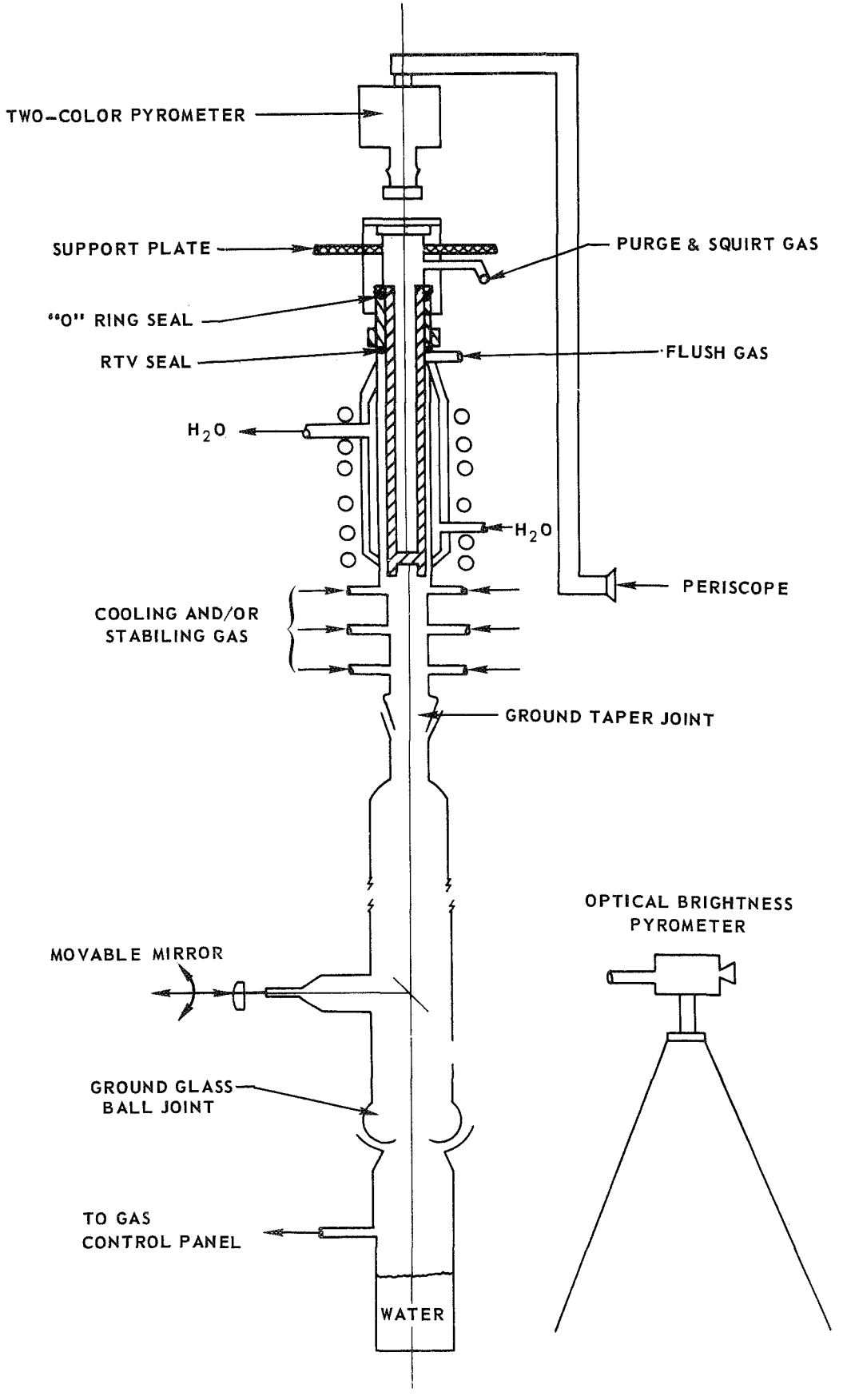

Experimental Results

The major variables in the process, the exit orifice design, the squirting pressure, and the temperature of the melt all interact to affect one another so that a discussion of the effects of these variables is difficult to separate into individual categories. However, since the orifice during any run is fixed and the other parameters are variable, this discussion will be based on a given orifice design with the effects of squirting pressure and temperature on the resultant oxide stream. The goal throughout the program was to obtain a long, stable, laminar stream of molten aluminum oxide that could be solidified into a fiber. The effects of jet turbulence as previously discussed were felt to be of paramount importance and, therefore, a great deal of effort was spent on obtaining laminar streaming through the orifice. The initial squirting runs were made with NASA specified orifices of 0.010 inch diameter, L/D approximately 1:1 and with entrance angles of 60° (see Fig. 4). Although the molten aluminum oxide squirted, some divergence of the flow was apparent. Bending calculations based on room temperature mechanical properties of the molybdenum orifice plate and 30 psig squirting pressure indicated that a 0.003 inch deflection would take place at room temperature; considerably more bending was to be expected at 2000°C. It was felt, therefore, that the deflection of the orifice plate with subsequent distortion of the circular orifice could account for the observed divergence of the molten stream during the squirting. To confirm the orifice plate deflection, a closed end nozzle was run with a typical charge and pressure (30 psig) applied at the same temperature as in the normal squirting experiments. The charge was solidified under pressure and the crucible cut open to permit observation of the bottom surface of the aluminum oxide. The deflection of the orifice plate can be seen by observing the "bowed" surface of the alumina as shown in Fig. 11. The actual deflection was measured to be 0.030 inches.

FIG. 11

SOLIDIFIED ALUMINUM OXIDE CHARGE

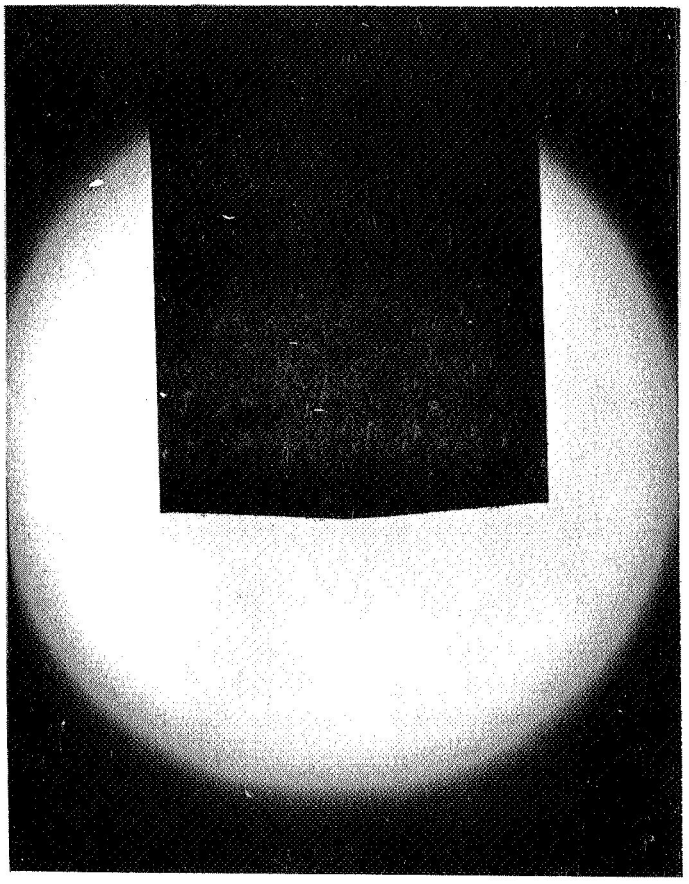

MAG. 5X

NOTE: EFFECT OF ORIFICE PLATE "BOWING"

Several squirt experiments were made with 0.0135 inch, 0.020 inch, and 0.040 inch thick orifice plates with a constant orifice diameter of 0.016 inch and a squirt pressure of 10 psig. The 0.040 inch thick orifice plate produced a good, straight stream of aluminum oxide and showed no visible deflection after squirting, whereas the 0.013 inch and 0.020 inch thick plates produced deflected streams even at the low 10 psi squirt pressure used for these experiments.

A series of experiments were run with 0.040 inch thick orifice plates at 5, 10, and 20 psi squirt pressures. Stable stream lengths were still short and no fiber was obtained at any of the squirting conditions. It was concluded at this time that the orifice plate design was still not correct and the effort was, therefore, concentrated on factors concerned with producing stable flow conditions.

If all the molten fluid in the crucible behaved as a perfect liquid at the instant of application of the squirting pressure, the entire container could have been fluid mechanically treated with a circular pipe flow model (Ref. 12). Since perturbations were present, such as a lower temperature gas contacting the top surface of the melt causing adverse thermal gradients and slight irregularities in wall thickness providing nonuniform heating, the assumption of fully developed flow in the body of the nozzle was not justified. In order to apply the Hagen-Poiseuille equations of flow through a pipe so that an analytically determined uniform velocity profile (Ref. 13) would enter the inlet to the exit orifice, thick orifice plates with nozzle details as shown in Fig. 12 were made. A pipe inlet diameter ratio of 8:1 was provided just prior to the entrance of the exit orifice to establish the desired laminar velocity profile.

To determine the geometric physical parameters for the orifice that would yield the least chance of falling within the turbulent flow regions, Reynold's number calculations were made. Each item in the Reynold's number definition was given a wide range of variance. The viscosity of molten aluminum oxide was allowed to

FIG. 12

THICK LAMINAR INLET ORIFICE PLATES

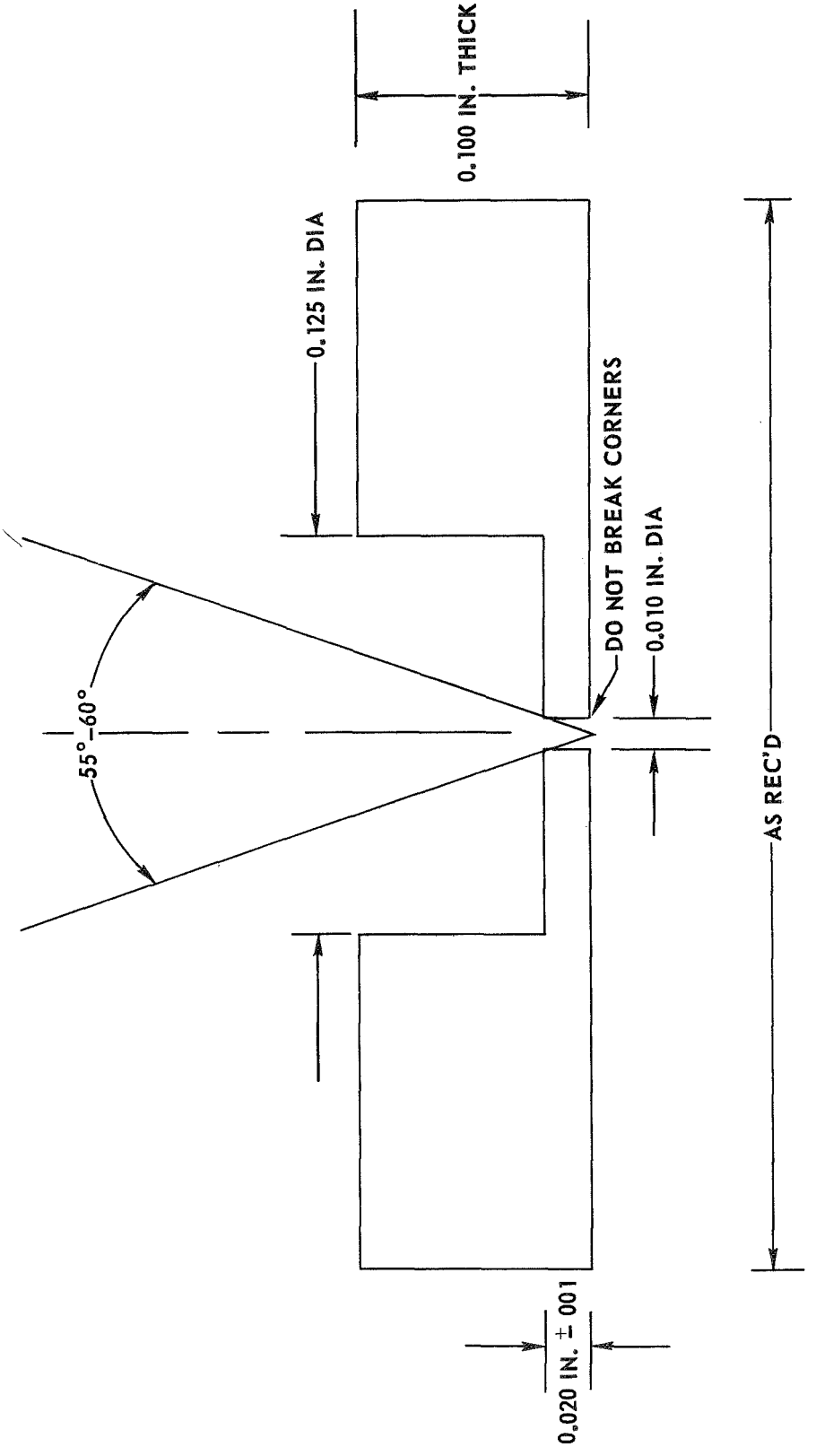

vary from 1 to 1000 centipoise. The orifice diameters ranged from 0.002 to 0.030 inch and the flow velocity varied from 1 to 1000 feet per second. The density of molten aluminum oxide at 2100°C (5.82 slugs/ft^3) was chosen for all calculations. The results are shown as Reynold's number versus velocity for various viscosities in Figs. 13 through 19. There is a Reynold's number plot for each orifice diameter from .002 inch up to .030 inch.

Simplified flow calculations assuming isotropic nozzle conditions (Ref. 14) were also made to determine the range of flow velocities for various squirting pressures. The actual stream velocities of the molten aluminum oxide and selected aluminum oxide alloys were then measured from high-speed movies taken of the experimental squirts. These measured velocities together with the calculated velocities were combined with newly obtained (Ref. 15) viscosity data to compress the field of calculable Reynold's numbers. The viscosity range used was 60 to 80 centipoise. The flow velocity was varied from 1 to 30 ft/sec.

The results are plotted as Reynold's number versus velocity for various viscosities in Figs. 20 through 26. There is again a Reynold's number plot for each orifice diameter. The same Reynold's number data are presented as functions of orifice diameter for various velocities at a constant viscosity in Figs. 27 through 31. A field plot is, therefore, available for viscosity values of 60, 65, 70, 75, and 80 centipoises.

With the experimentally measured velocities, known jet diameter and reasonably close viscosity values, the Reynold's number data showed that the laminar flow region prevailed for most all conditions employed in our experiments.

Fastax motion pictures at 1000 frames per second were taken of many squirt experiments using the thick laminar inlet orifice plate and indicated that the stable jet length was increased from the initial 1/2 inch to approximately 3 inches. Aluminum oxide fibers 0.005 inch to 0.010 inch in diameter and up to

FIG. 13

REYNOLDS NUMBER VS VELOCITY FOR VARIOUS VISCOSITIES (CENTIPOISE)

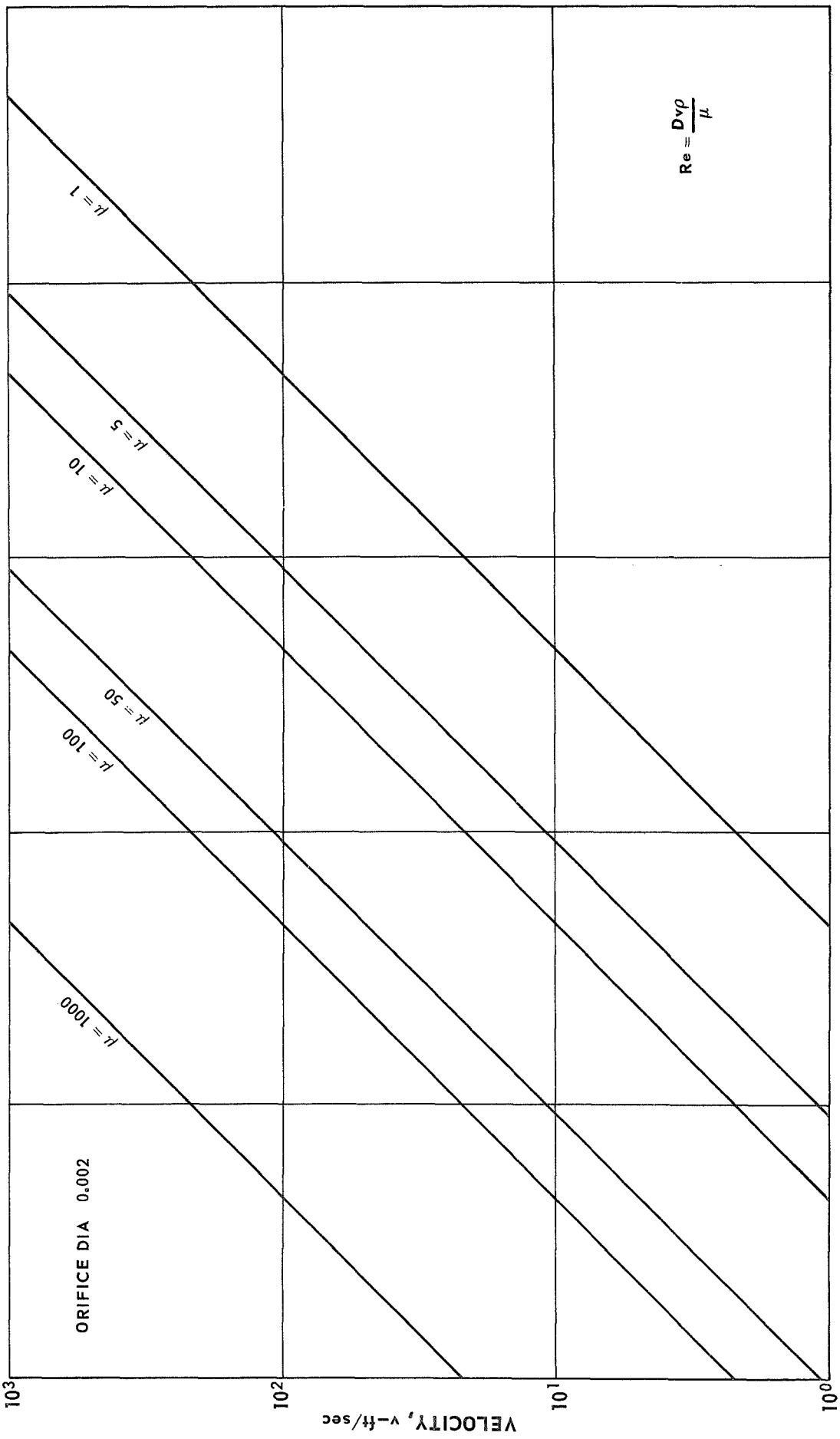

FIG. 14

REYNOLDS NUMBER VS VELOCITY FOR VARIOUS VISCOSITIES (CENTIPOISE)

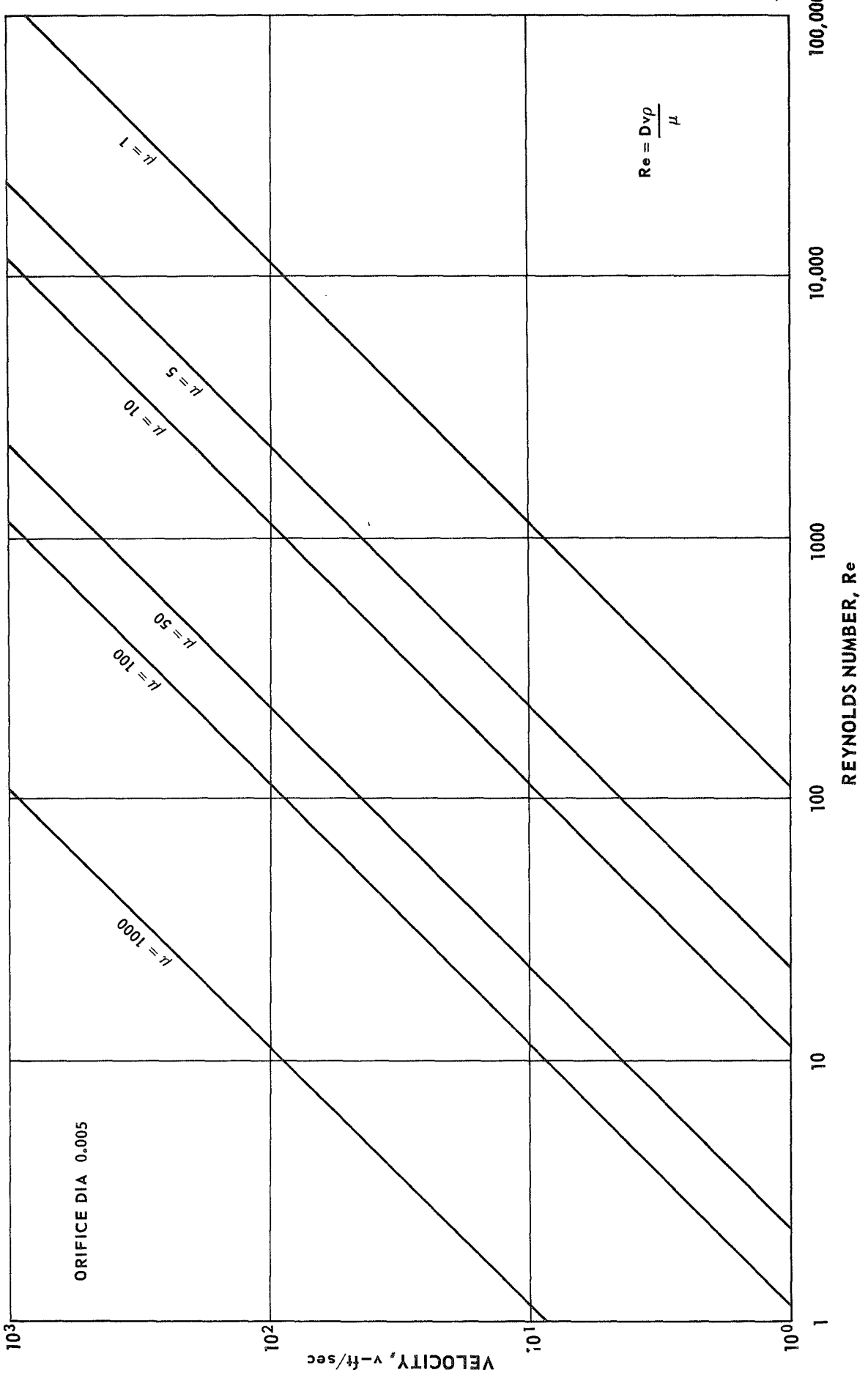

FIG. 15

REYNOLDS NUMBER VS VELOCITY FOR VARIOUS VISCOSITIES (CENTIPOISE)

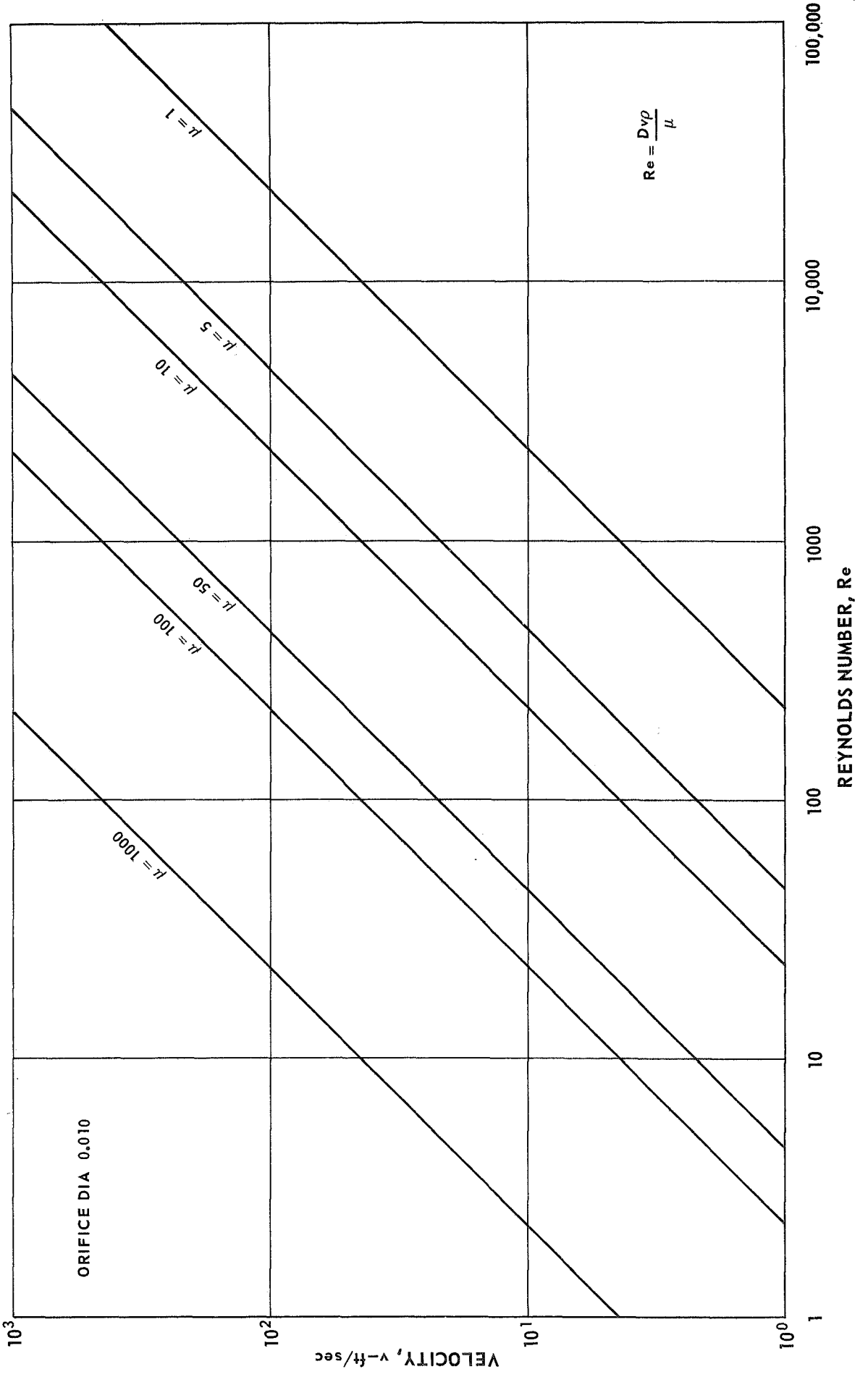

FIG. 16

REYNOLDS NUMBER VS VELOCITY FOR VARIOUS VISCOSITIES (CENTIPOISE)

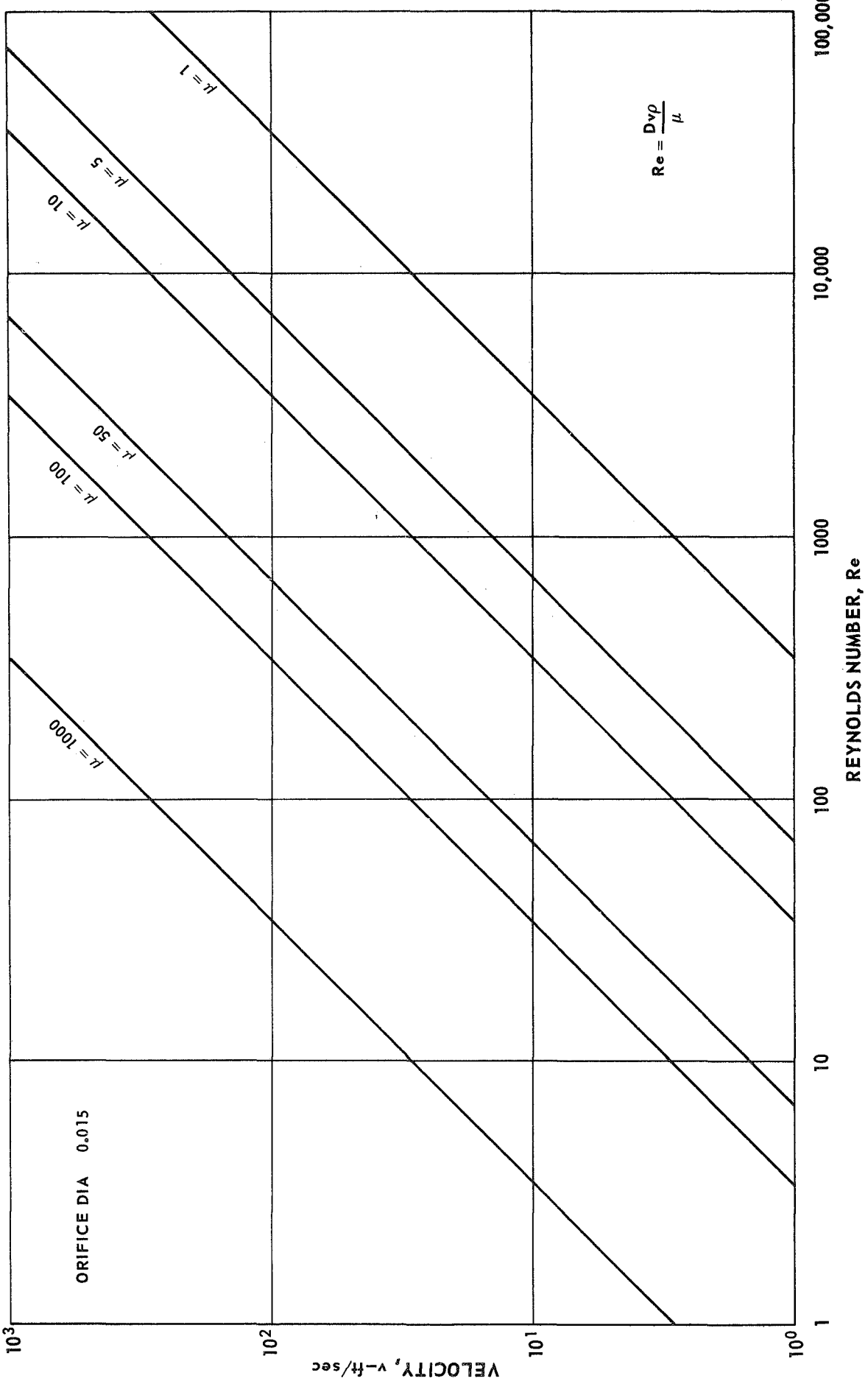

FIG. 17

REYNOLDS NUMBER VS VELOCITY FOR VARIOUS VISCOSITIES (CENTIPOISE)

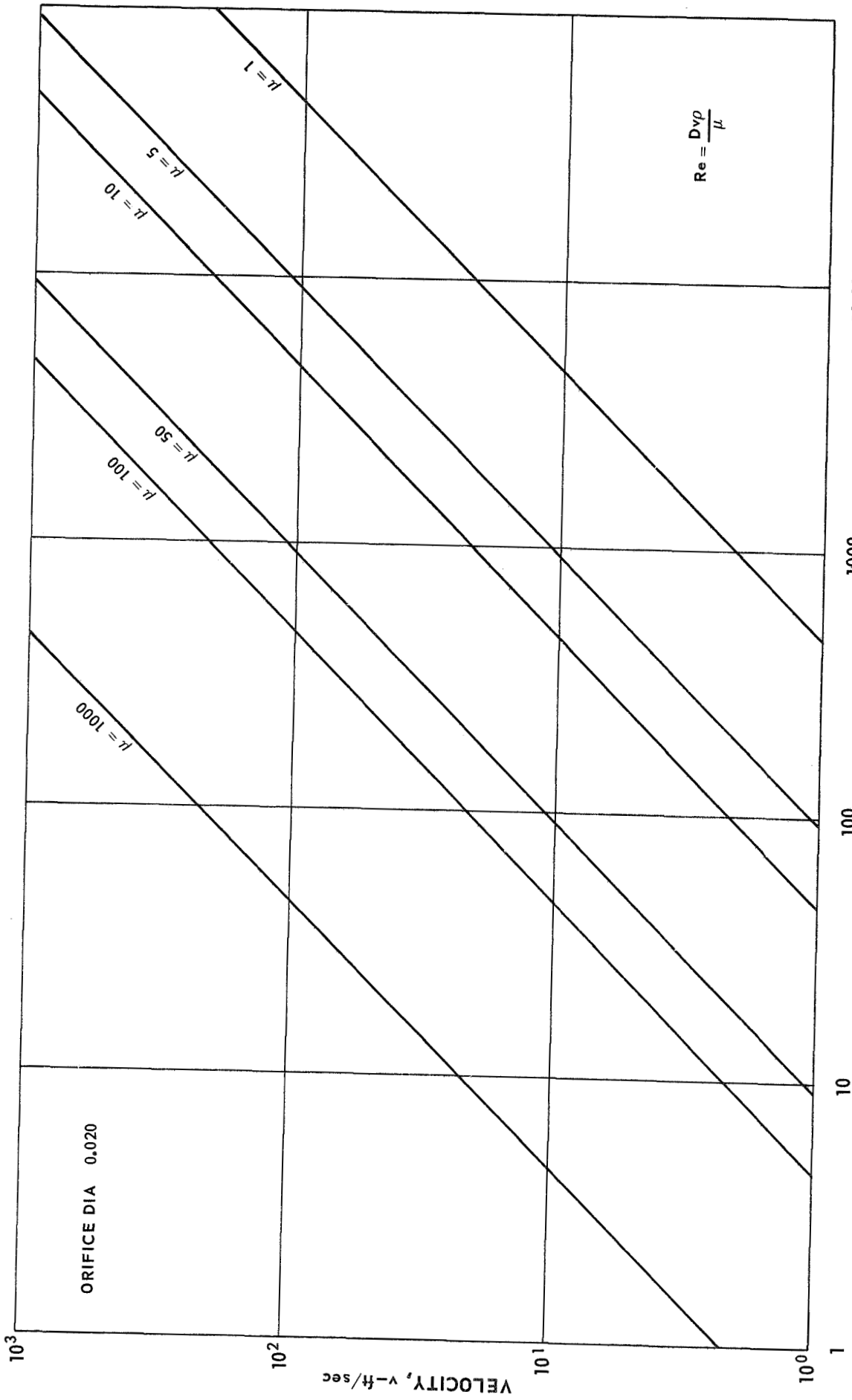

FIG. 18

REYNOLDS NUMBER VS VELOCITY FOR VARIOUS VISCOSITIES (CENTIPOISE)

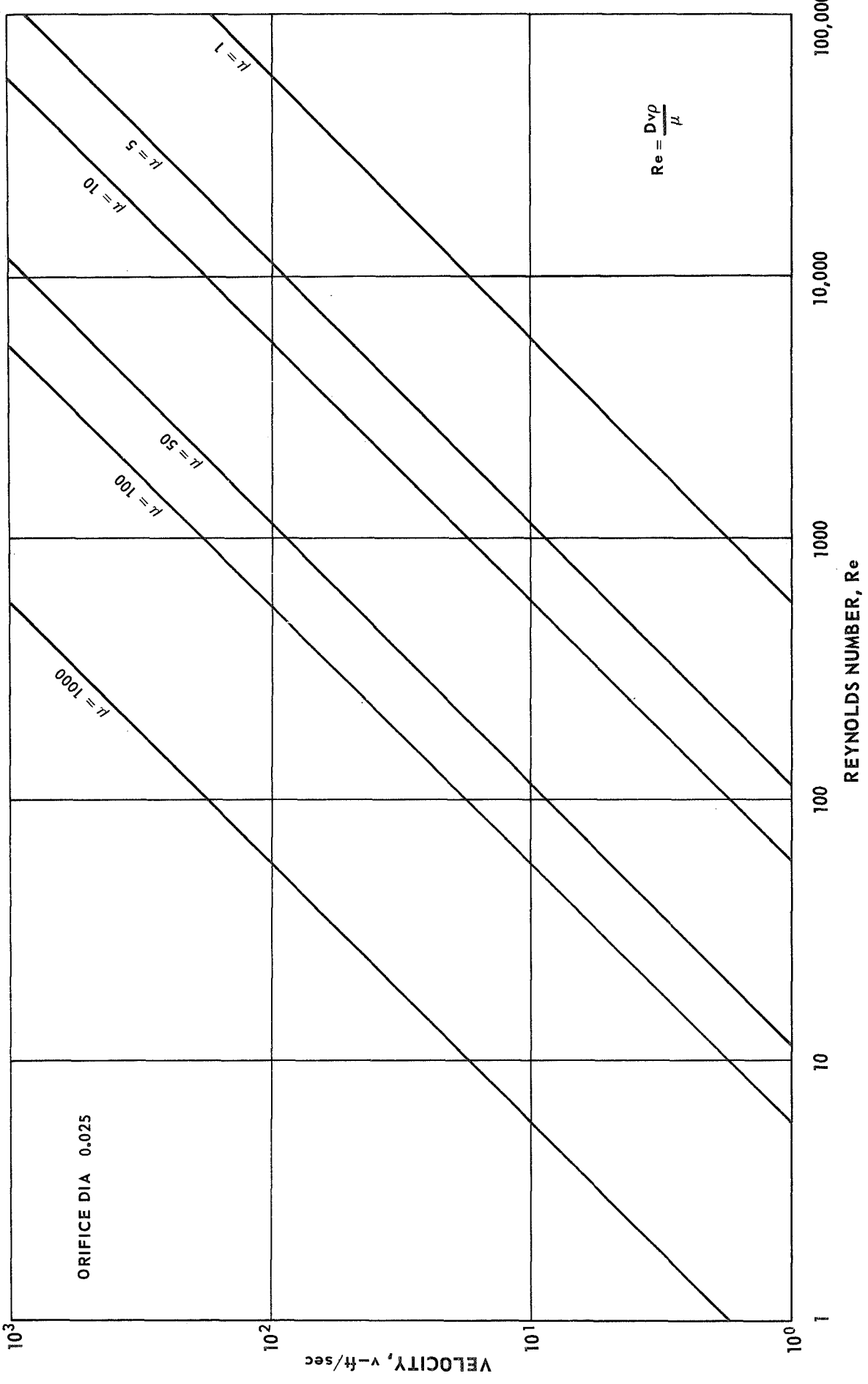

FIG. 19

REYNOLDS NUMBER VS VELOCITY FOR VARIOUS VISCOSITIES (CENTIPOISE)

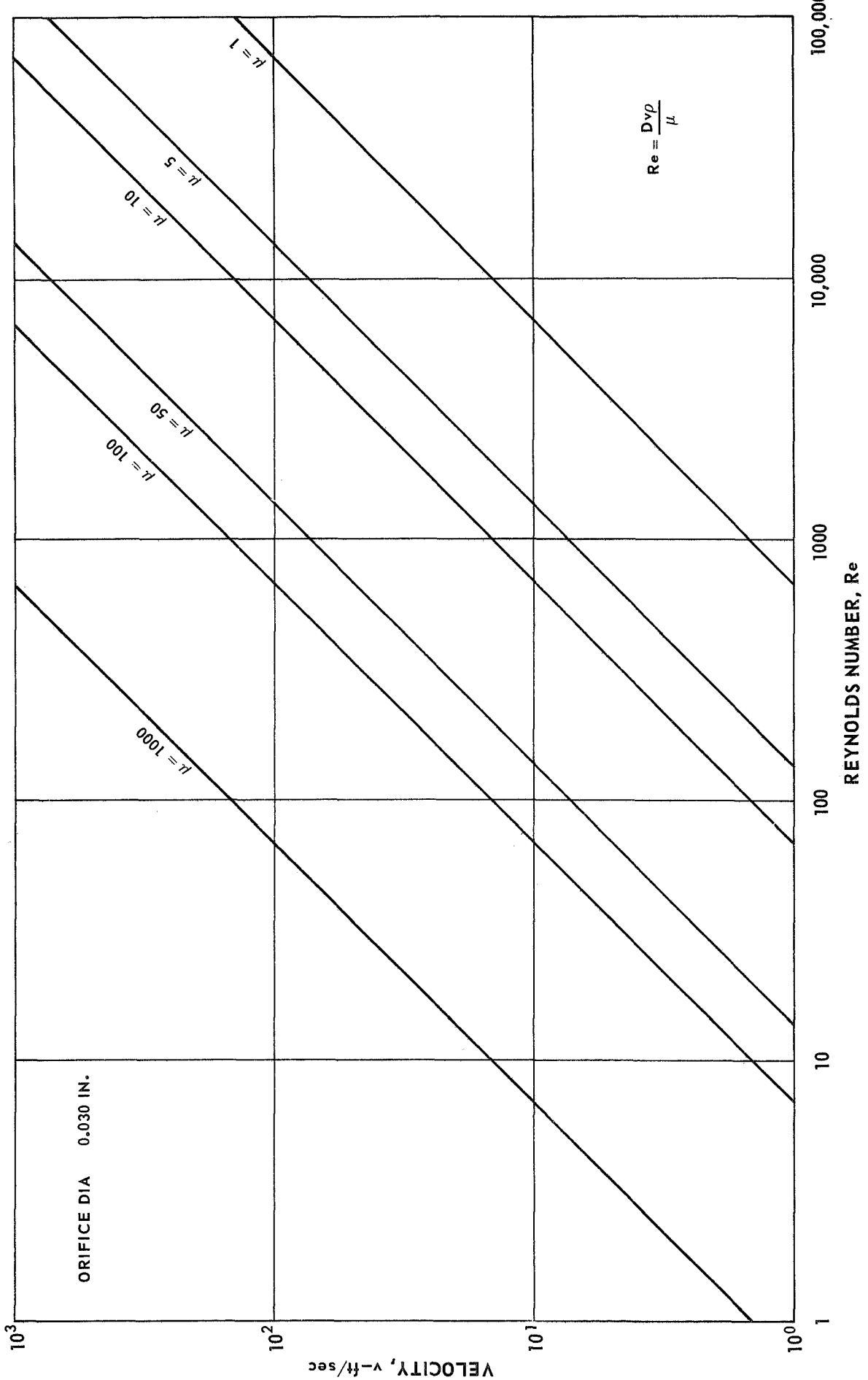

FIG. 20

REYNOLDS NUMBER VS VELOCITY FOR VARIOUS VISCOSITIES (CENTIPOISE)

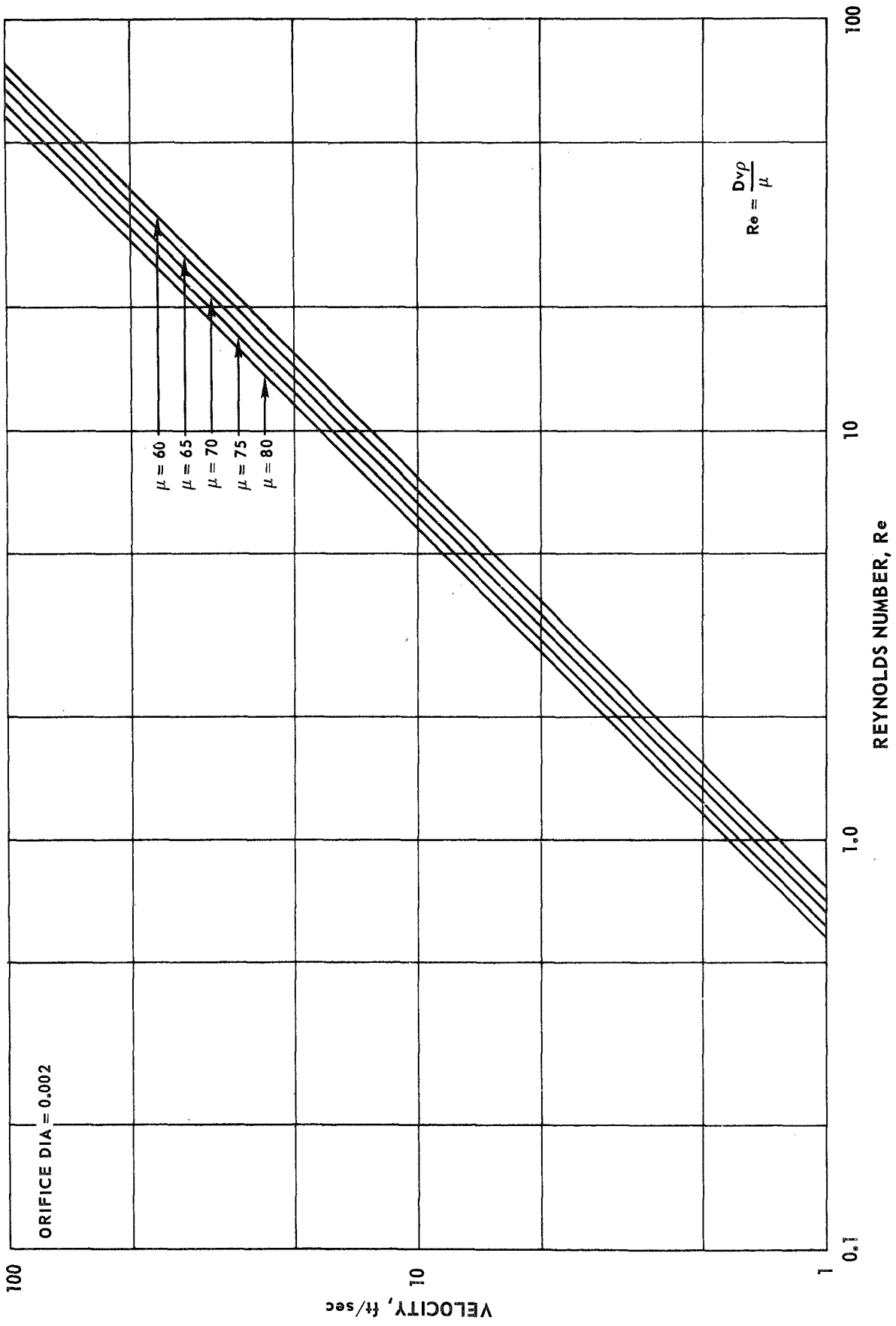

FIG. 21

REYNOLDS NUMBER VS VELOCITY FOR VARIOUS VISCOSITIES (CENTIPOISE)

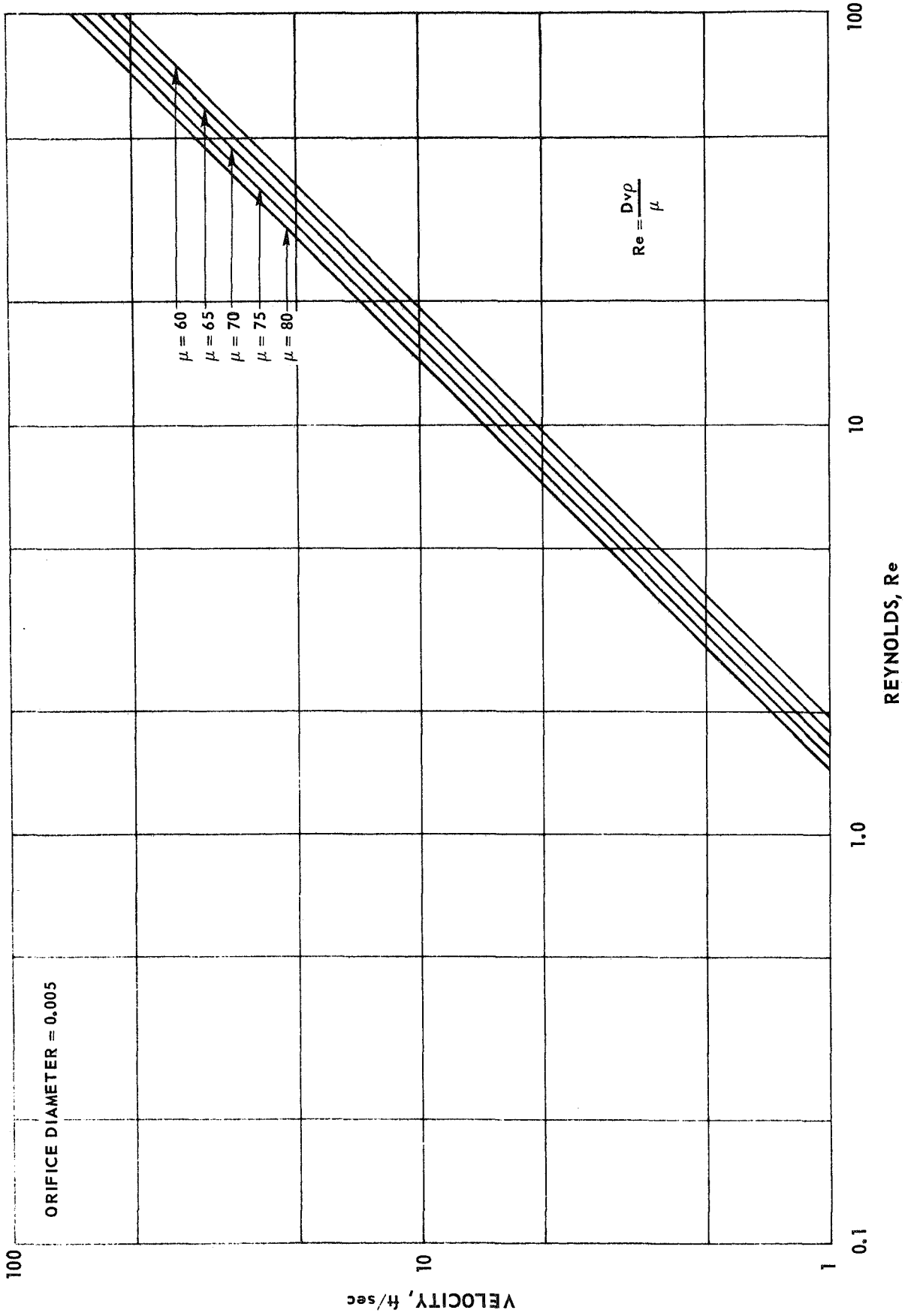

FIG. 22

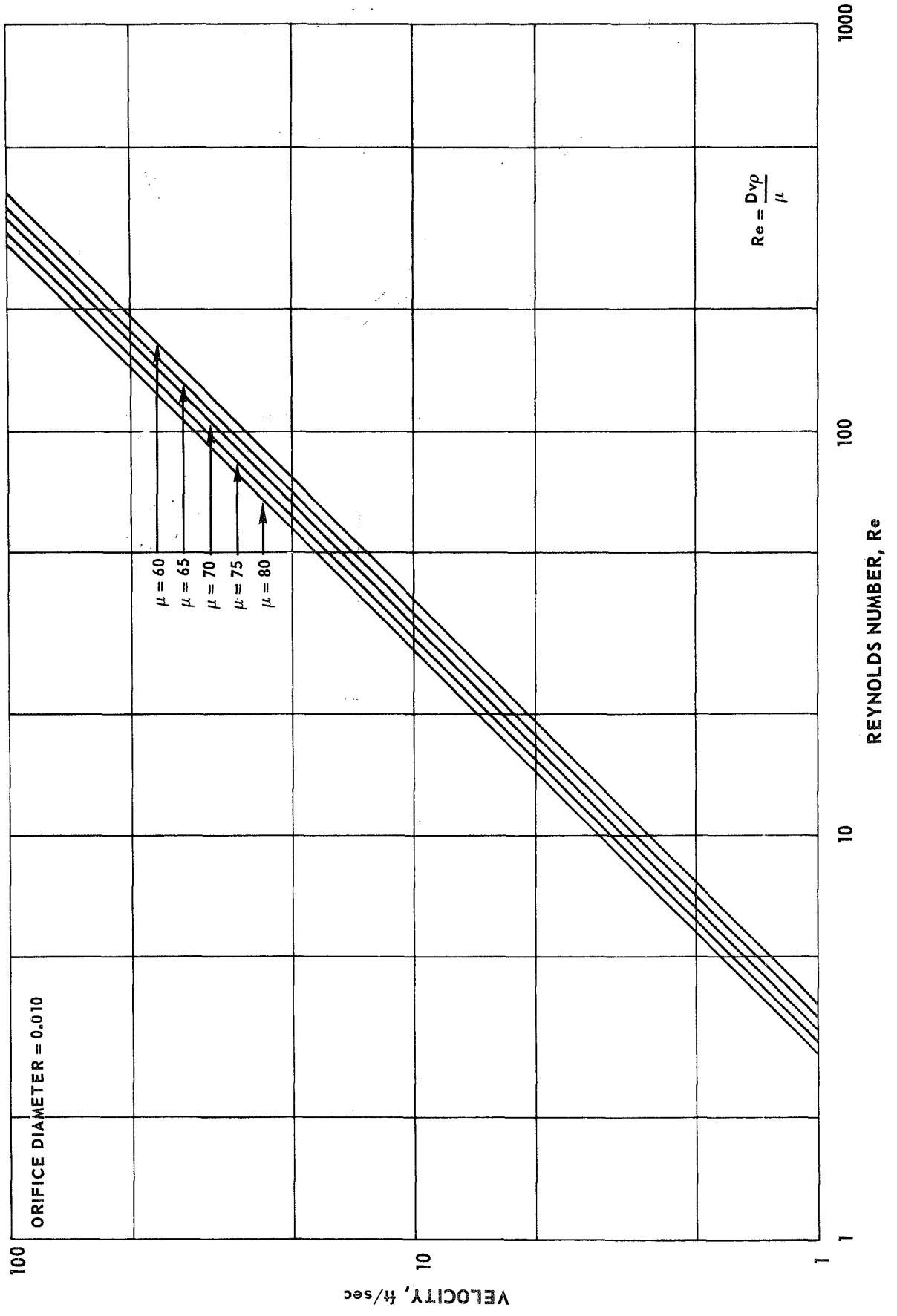
REYNOLDS NUMBER VS VELOCITY FOR VARIOUS VISCOSITIES (CENTIPOISE)
ORIFICE DIAMETER = 0.010
$\mu = 60$
$\mu = 65$
$\mu = 70$
$\mu = 75$
$\mu = 80$
$Re = \frac{Dv\rho}{\mu}$
VELOCITY, ft/sec
100
10
1
REYNOLDS NUMBER, Re
1000
100
10
1

FIG. 23

REYNOLDS NUMBER VS VELOCITY FOR VARIOUS VISCOSITIES (CENTIPOISE)

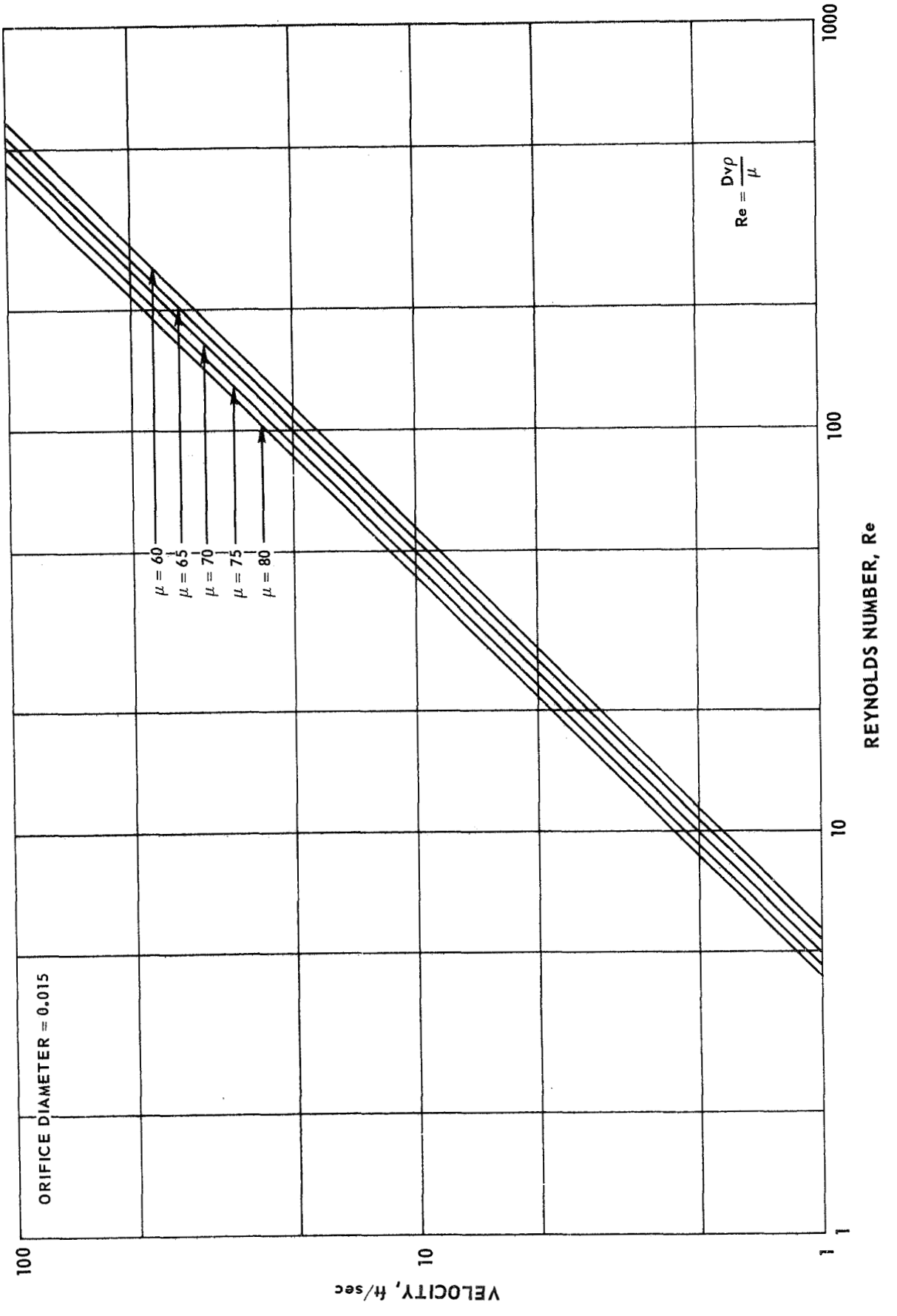

FIG. 24

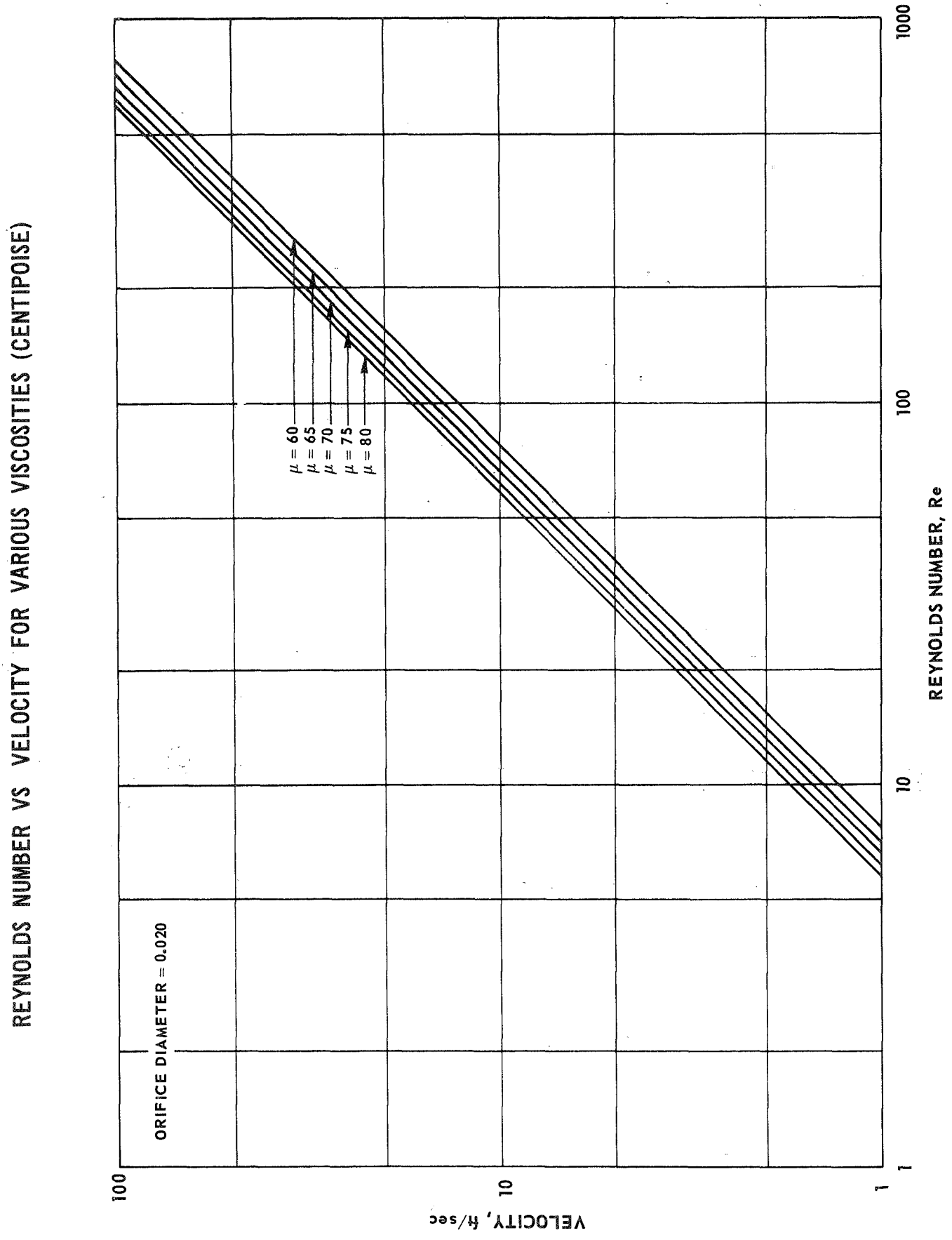
REYNOLDS NUMBER VS VELOCITY FOR VARIOUS VISCOSITIES (CENTIPOISE)
ORIFICE DIAMETER = 0.020
$\mu = 60$
$\mu = 65$
$\mu = 70$
$\mu = 75$
$\mu = 80$
VELOCITY, ft/sec
100
10
1
REYNOLDS NUMBER, Re
1000
100
10
1

FIG. 25

REYNOLDS NUMBER VS VELOCITY FOR VARIOUS VISCOSITIES (CENTIPOISE)

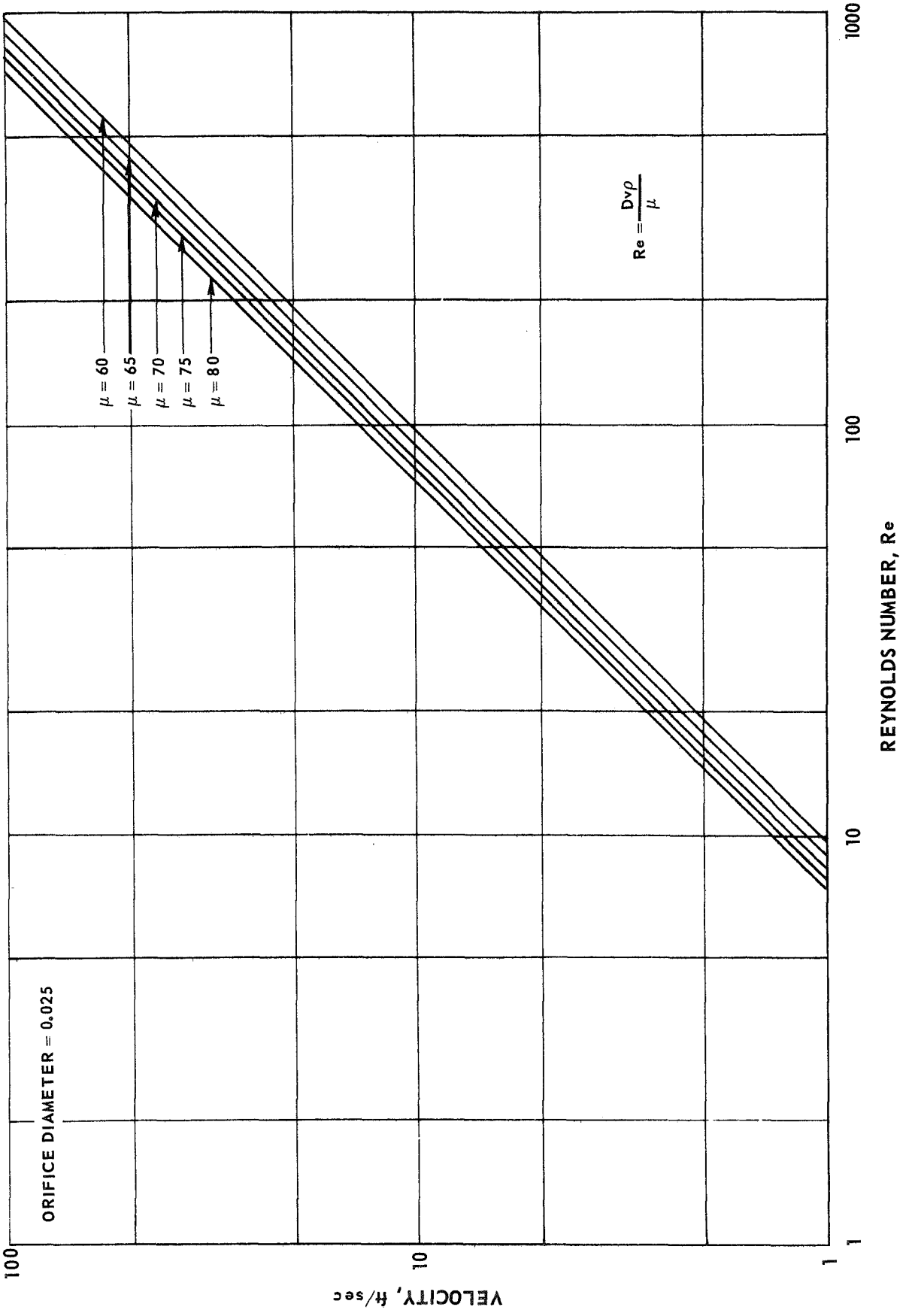

FIG. 26

REYNOLDS NUMBER VS VELOCITY FOR VARIOUS VISCOSITIES (CENTIPOISE)

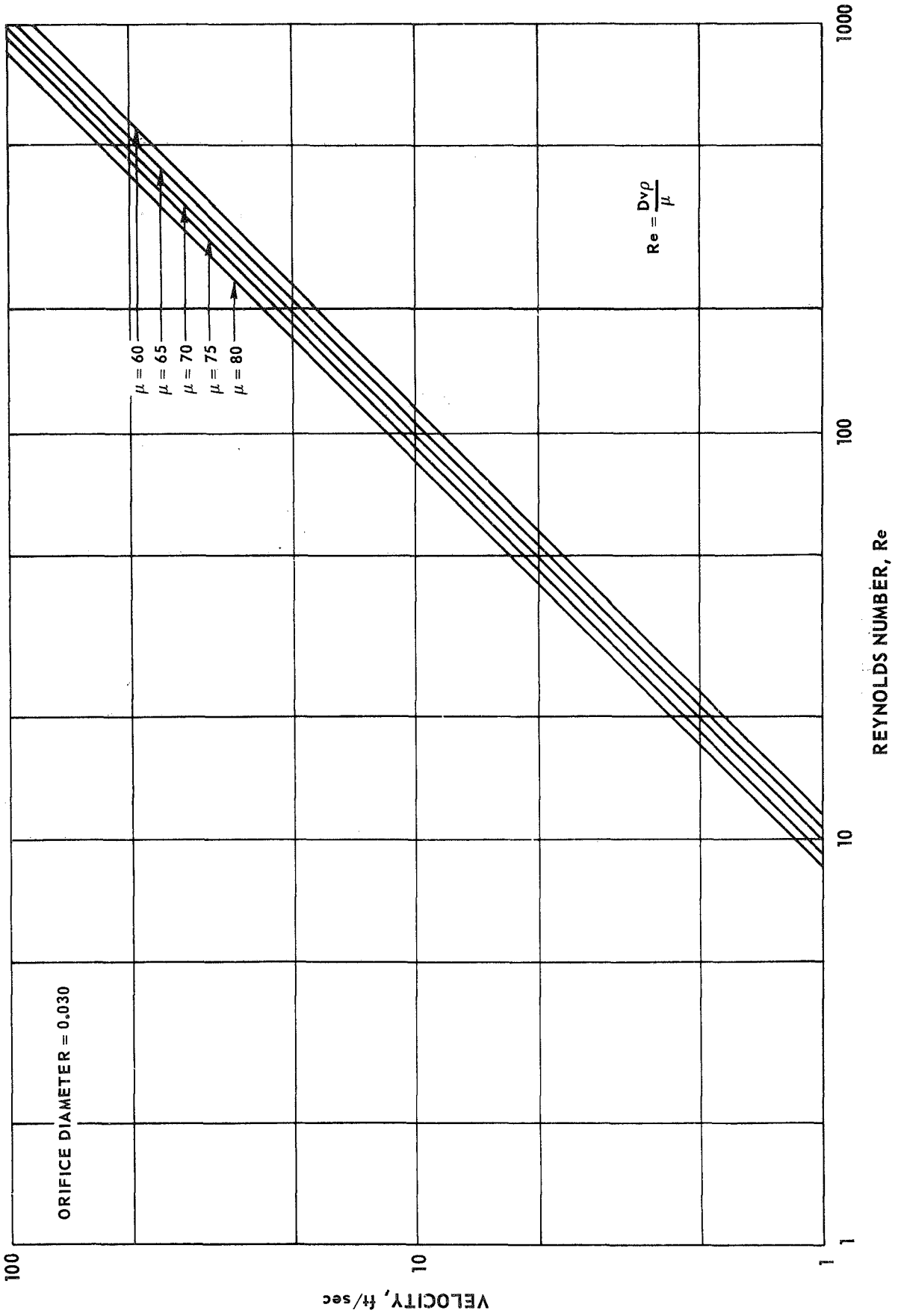

FIG. 27

REYNOLDS NUMBER VS. ORIFICE DIAMETER FOR VARIOUS VELOCITIES

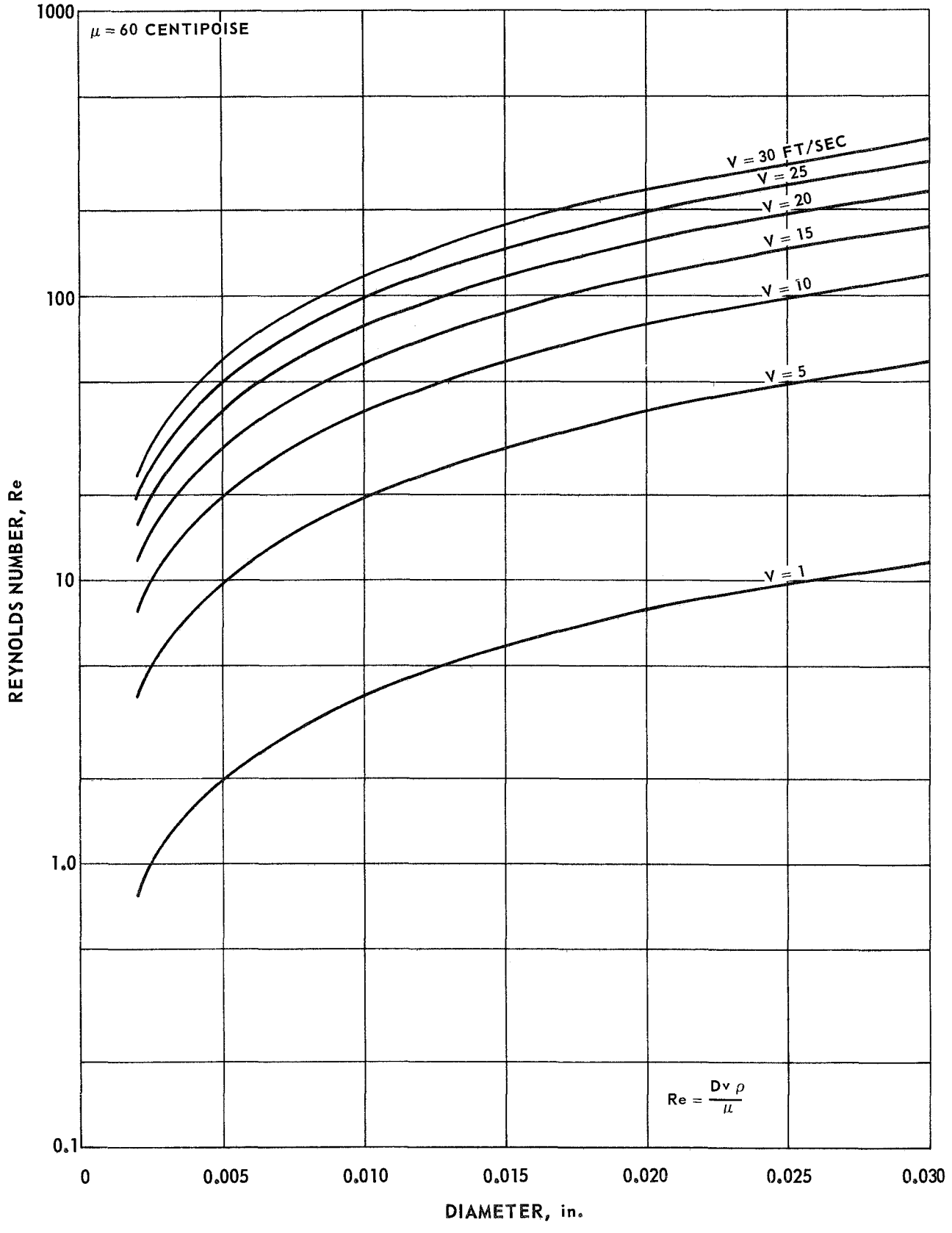

FIG. 28

REYNOLDS NUMBER VS. ORIFICE DIAMETER FOR VARIOUS VELOCITIES

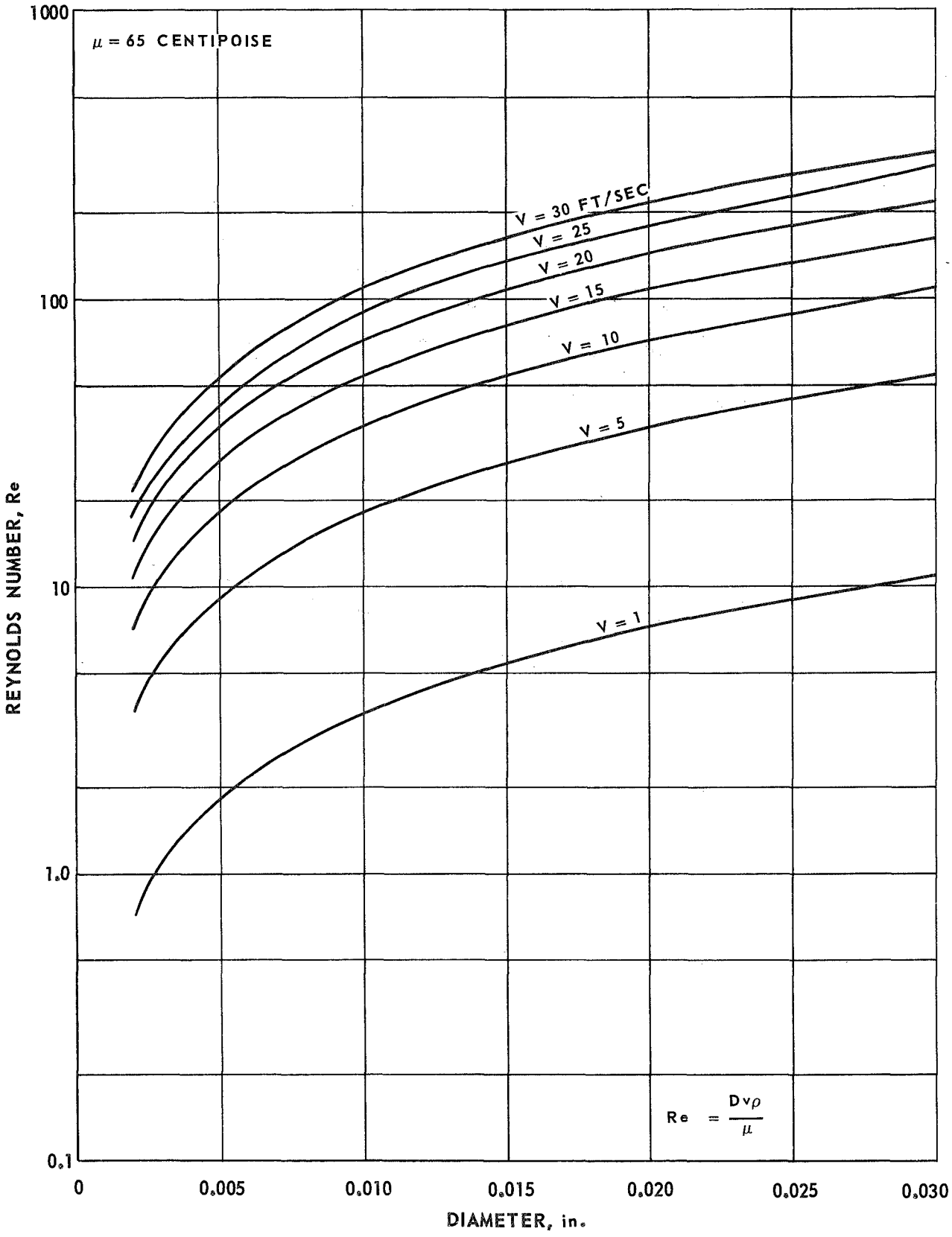

FIG. 29

REYNOLDS NUMBER VS. ORIFICE DIAMETER FOR VARIOUS VELOCITIES

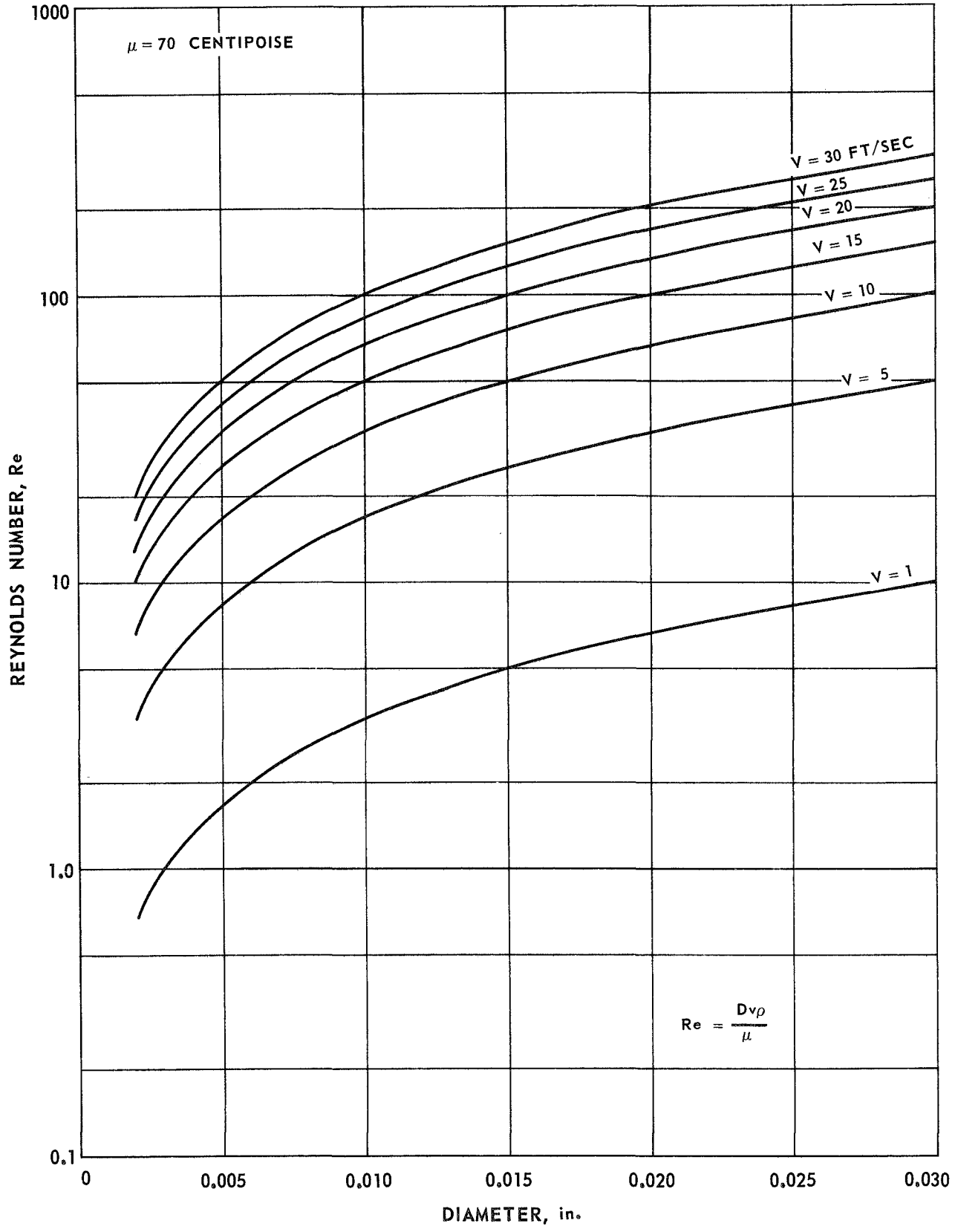

FIG. 30

REYNOLDS NUMBER VS. ORIFICE DIAMETER FOR VARIOUS VELOCITIES

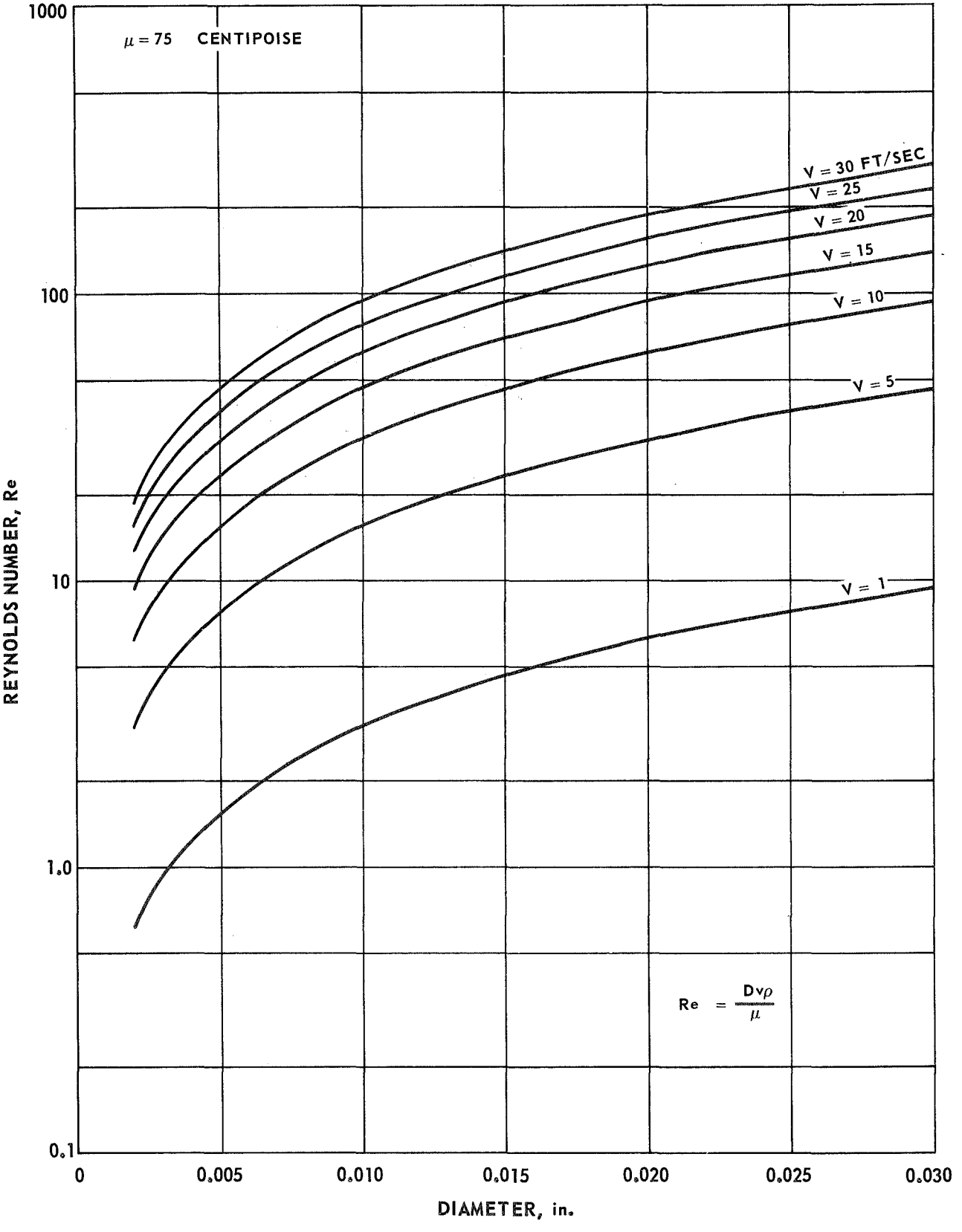

FIG. 31

REYNOLDS NUMBER VS. ORIFICE DIAMETER FOR VARIOUS VELOCITIES

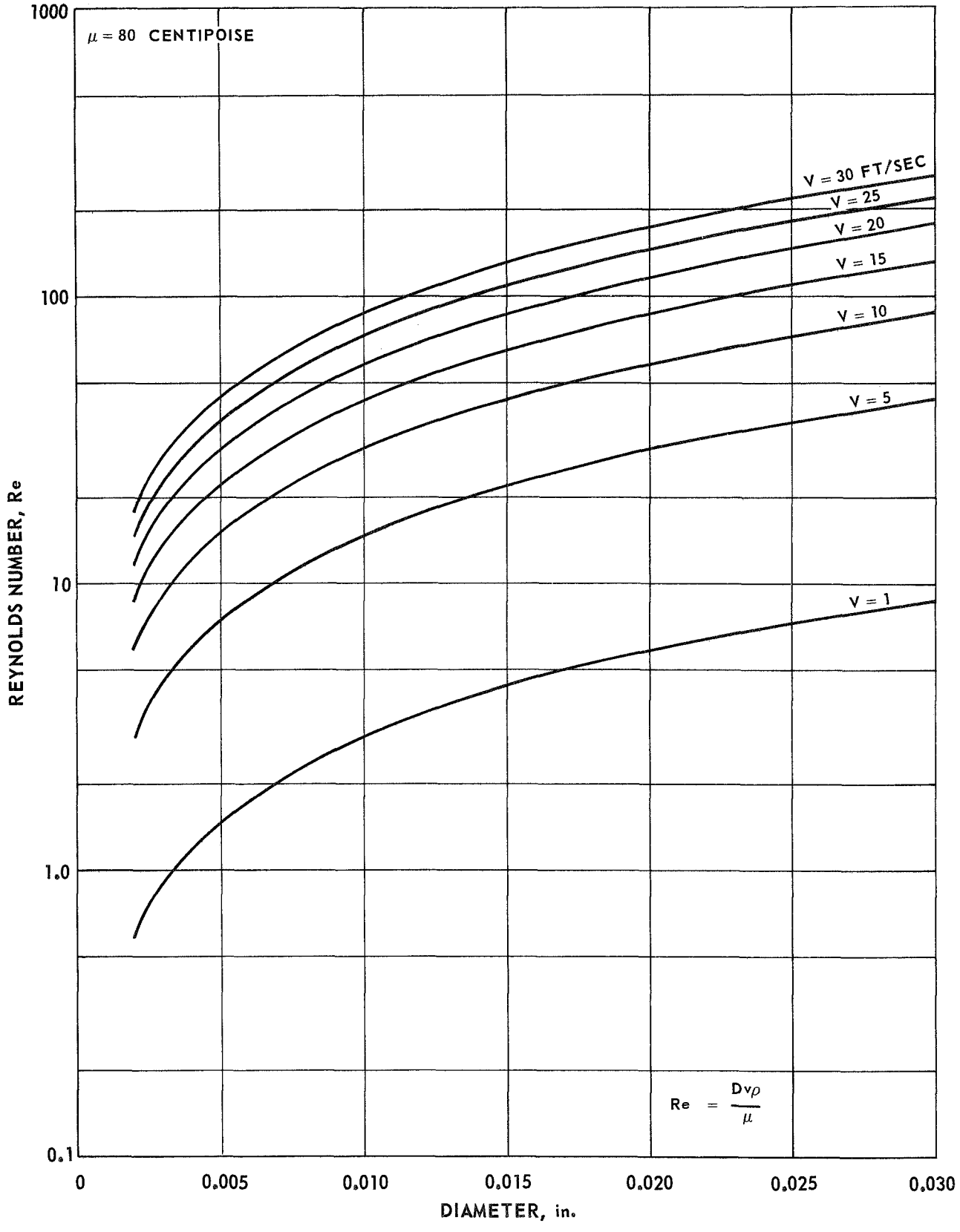

1/4 inch long were produced during these experiments. Figure 32 shows some typical fibers from these runs. Although the fibers were too small for mechanical testing, X-ray analysis indicated that these fibers were α-aluminum oxide.

All attempts to solidify the stable jet into a continuous fiber were unsuccessful. The transverse coolers were not effective, probably because the space limitations on the equipment did not allow them to be placed close enough to the orifice exit. The transverse flow principle was proven, however, inasmuch as no stream deflection took place under high cooling gas flows.

Squirting experiments with the alloy oxide systems showed that their behavior was not different from that of the pure aluminum oxide.

Attempts to utilize ammonia and methane as stabilizing media were unsuccessful. This work was inconclusive in that high volume percentages of these gases could not be used due to the danger of explosion in the glass-enclosed equipment used for these experiments.

CONCLUSIONS

Although only short fibers of both aluminum oxide and aluminum oxide alloys have been produced under this program, the results indicate that aluminum oxide can be squirted through small orifices with a stable jet length of approximately three inches. Also, since the gas-cooling experiments have shown that a transverse gas flow does not appreciably alter the path of the molten stream, it should be possible to solidify the jet into a continuous filament of aluminum-oxide with suitably placed transverse coolers.

There does not yet appear to be any advantage in using the oxide alloys over pure aluminum oxide. Metallographic examination of shot produced from several experiments showed that aluminum oxide and aluminum oxide alloys both produced

FIG. 32

MELT SPUN ALUMINUM OXIDE FIBERS

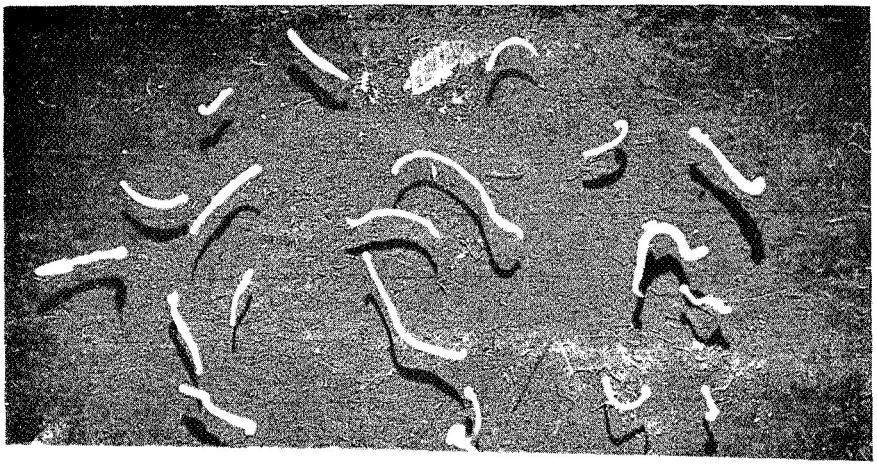

MAG: 4X

about the same amount of hollow spheres; the use of the alloy additions to the melt did not, therefore, appear to change the distribution of shrinkage cavities during solidification. No correlation could be found between the void size (Figs. 33,34) and the diameter of the spheres.

Stabilization of a molten jet of aluminum oxide may be possible using high-volume percentages of reactant gases in the squirting environment. These percentages should be in excess of 20 percent and the gas must be introduced as close to the orifice exit as possible without causing plugging of the nozzle.

SUGGESTIONS FOR FUTURE WORK

Since very little difficulty was experienced in obtaining good streaming of the aluminum oxide once the correct orifice plate design was found, any future work using a melt spinning technique should concentrate upon stream cooling, surface tension control, and stream stabilization. The use of other gases as squirting environments may result in a lower interfacial tension of the aluminum oxide which will allow solidification of the stream before it breaks up into shot.

Alloy additions (in small amounts) of high melting oxides such as HfO_2 and ZrO_2 may be effective in increasing the solidification rate of the molten stream.

A promising technique that should also be explored in any future work is the production of aluminum oxide ribbon by splat cooling the molten jet against a cold rotating drum. If the drum were to be placed very near the orifice exit, it would be in the stable stream zone and a continuous ribbon of aluminum oxide should be formed.

FIG. 33

CROSS SECTION OF SOLID TADPOLE OF ALUMINUM OXIDE

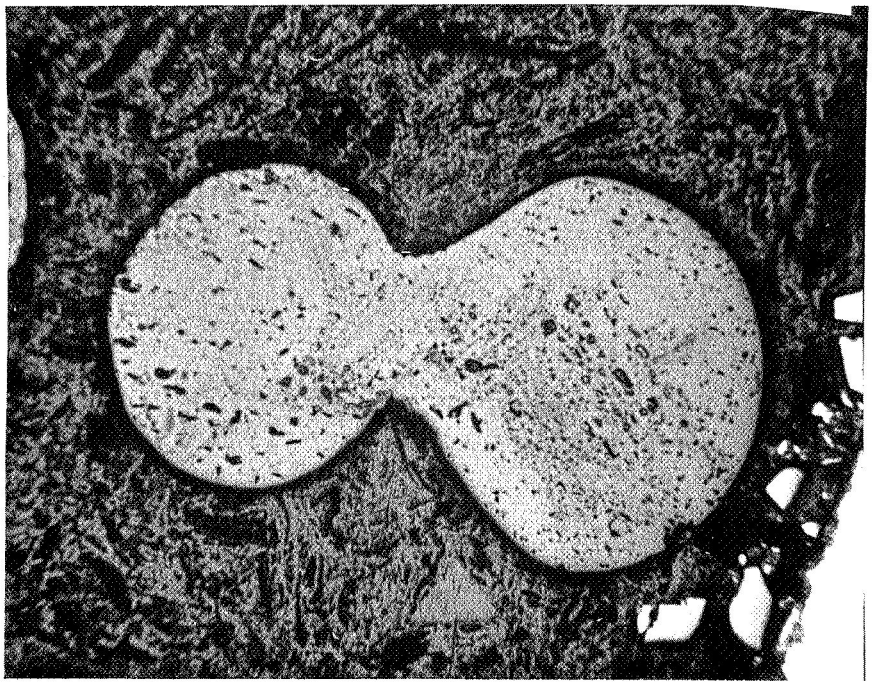

100X

CROSS SECTION OF ALUMINUM OXIDE SHOT

(NOTE VOIDS)

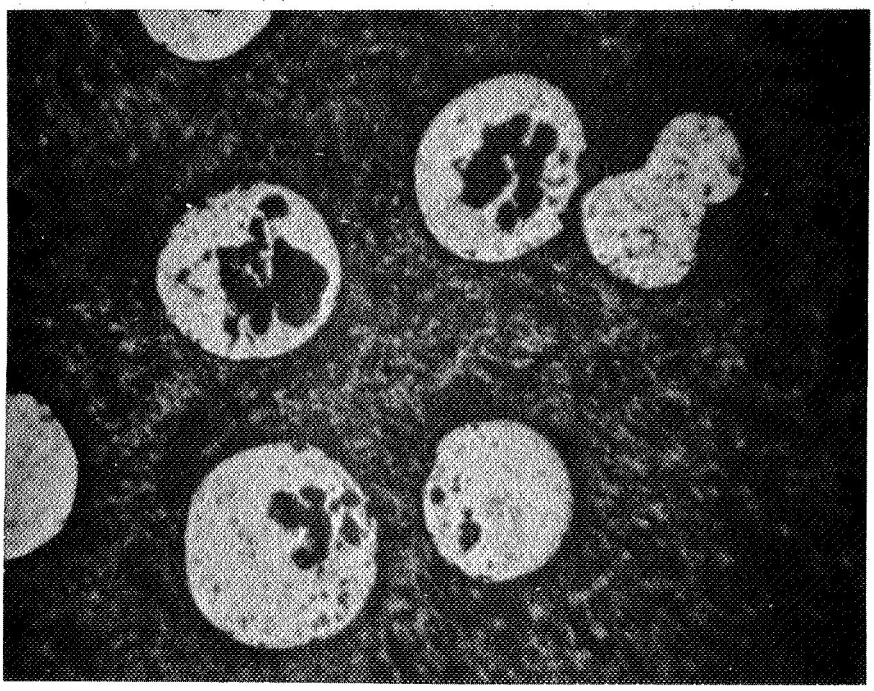

50X

REFERENCES

1. Chandresekhar, S.: Hydrodynamic and Hydromagnetic Stability. Clarendon Press, Oxford, 1961.

2. Gupta, A. S.: On the Capillary Instability of a Jet Carrying an Axial Current With or Without a Longitudinal Magnetic Field. Proceedings of the Royal Society, Vol. 278, No. 1373, March 24, 1964.

3. Schweitzer, P. H.: Mechanism of Disintegration of Liquid Jets. Jl. of Applied Physics, Vol. 8, No. 8, p. 513, August 1937.

4. Kozakevitch, P. and Georges Urbain: Tension Superficielle du fer Liquide et de Ses Alliages. Memoires Scientifiques Rev. Mettalurg.

   Part I - Vol. 58, No. 6, 1961
   Part II - Vol. 58, No. 7, 1961
   Part III - Vol. 58, No. 12, 1961

5. Strauss, S. W.: An Empirical Surface Tension-Temperature Relation for Liquid Metals. Reactor Science and Technology, Vol. 15, p. 28, 1961.

6. Strauss, S. W.: The Surface Tensions of Liquid Metals at Their Melting Points. Nuclear Science and Engineering, Vol. 8, No. 4, p. 362, 1960.

7. Rare Metals Handbook. Reinhold Publishing Corp., p. 74.

8. Bergwerk, W.: Flow Patterns in Diesel Nozzle Spray Holes. Proc. Instr. Mech. Engrs., Vol. 173, No. 25, p. 655, 1959.

9. Spikes, R. H. and G. A. Pennington: Discharge Coefficient of Small Submerged Orifices. Proc. Instr. Mech. Engrs., Vol. 173, No. 25, p. 661, 1959.

10. Carley, C. T.: Experiments on Transition Regime Flow Through a Short Tube with a Bellmouth Entry. AIAA Journal, Vol. 4, No. 1, p. 47, Jan. 1966.

11. Panasenkov, N. S.: The Effect of Turbulence of a Jet on Its Dispersion. Zhurnal Technicheskii Phyzik, Vol. 21, No. 2, p. 160, Feb. 1951 (in Russian).

12. Kays, W. M.: Convective Heat and Mass Transfer. McGraw Hill, New York, p. 37, 1966.

13. Schlichting, H.: Boundary Layer Theory. McGraw Hill, New York, p. 68, 376, 1960.

14. Shapiro, A. H.: The Dynamics and Thermodynamics of Compressible Fluid Flow. Ronald Press, New York, Chapter 4, 1953.

15. Rasmussen, J. J., R. P. Nelson, and J. A. Christensen: Surface Tension and Density of Molten Alumina. American Ceramic Society Meeting, Paper No. 14-R-70, Philadelphia, Pa., May 1970.

DISTRIBUTION LIST

(Numbers in parentheses indicate number of copies to each addressee)

NASA Headquarters
Washington, D. C. 20546
Attn: N. F. Rekos (RAP) (1)
G. C. Deutsch (RW) (1)
R. H. Raring (RWM) (1)
J. J. Gangler (RWM) (1)

NASA Lewis Research Center
21000 Brookpark Road
Cleveland, Ohio 44135
Attn: Technology Utilization Office, MS 3-19 (1)
John Weeton, MS 49-1 (2)
G. M. Ault, MS 3-13 (1)
R. W. Hall, MS 105-1 (1)
Library, MS 60-3 (2)
Report Control Office MS 5-5 (1)
R. A. Signorelli, MS 106-1 (3)
L. J. Westfall, MS 106-1 (1)
A. E. Anglin, MS 106-1 (10)

FAA Headquarters
900 Independence Avenue, SW
Washington, D. C. 20553
Attn: Brig. Gen. J. C. Maxwell (1)

NASA Scientific and Technical Information Facility (6)
P.O. Box 33
College Park, Maryland 20740

U.S. Atomic Energy Commission
Washington, D. C. 20545
Attn: Technical Reports Library (1)
Jules Simmons (1)

Air Force Office of Scientific Research (1)
Propulsion Research Division
USAF Washington, D. C. 20525

Defense Documentation Center (1)
Cameron Station
5010 Duke Street
Alexandria, Virginia 22314

Headquarters
Wright-Patterson AFB, Ohio 45433
Attn: MAAM-Technical Library (1)
AFSC-FTDS (1)
AFML-A. M. Lovelace (1)
SESOS (1)

Department of the Navy
ONR - Code 429
Washington D. C. 20525
Attn: Dr. R. Roberts (1)

U. S. Army Aviation Materials Laboratory
Fort Eustis, Virginia 23604
Attn: John White, Chief, SMOFE-APG (1)

Chief, Bureau of Naval Weapons
Department of the Navy
Washington, D. C. 20525
Attn: T. F. Kearns (1)

NASA Langley Research Center
Langley Field, Virginia 23365
Attn: Library (1)
Richard Pride (1)

NASA Marshall Space Flight Center
Huntsville, Alabama 35812
Attn: Library (1)

Jet Propulsion Laboratory
4800 Oak Grove Drive
Pasadena, California 91102
Attn: Library (1)

Army Materials Research Agency
Watertown Arsenal
Watertown, Massachusetts 02172
Attn: S. V. Arnold, Director (1)

NASA Ames Research Center
Moffett Field, California 94035
Attn: Library (1)

NASA Goddard Space Flight Center
Greenbelt, Maryland 20771
Attn: Library (1)

NASA Manned Space Flight Center
Houston, Texas 77058
Attn: Library (1)

NASA Flight Research Center
P.O. Box 273
Edwards, California 93523
Attn: Library (1)

Defense Metals Information Center (1)
Battelle Memorial Institute
505 King Avenue
Columbus, Ohio 43201

General Electric Company
Advanced Technology Laboratory
Schenectady, New York 12305
Attn: Library (1)

General Electric Company
Materials Development Laboratory
Operation
Advanced Engine and Technology
Department
Cincinnati, Ohio 45215
Attn: L. P. Jahnke (1)

General Motors Corporation
Allison Division
Indianapolis, Indiana 46206
Attn: D. K. Hanink, Materials
Laboratory (1)

Stanford University
Palo Alto, California 94305
Attn: Prof. Oleg Sherby
Department of Material
Science (1)

United Aircraft Corporation
400 Main Street
East Hartford, Connecticut 06108
Attn: E. F. Bradley, Chief
Materials Engineering (1)

Lockheed Mississippi Space Co.
Palo Alto Research Laboratory
Palo Alto, California
Attn: J. L. Camahort (1)

NASA Langley Research Center
Langley Field, Virginia 23365
Attn: John Buckley (1)

One copy each to the following:

N. R. Adsit
General Dynamics/Convair
Mail Zone 572-10
P.O. Box 1128
San Diego, California 92112

Dr. I. Ahmad
Maggs Research Center
Watervliet Arsenal
Watervliet, New York 12189

J. Bartos
General Electric AETD
Evandale, Ohio 45215

H. P. Borie
Hamilton Standard Division
United Aircraft Corporation
Windsor Locks, Connecticut 06096

C. A. Calon
U.K.A.E.A.
Atomic Weapon Research Establishment
Aldermaston, Berkshire, England

J. L. Camahort
Lockheed Missile/Space Company
Palo Alto Research Laboratory
Palo Alto, California

Dr. W. H. Chang
General Electric AETD
Evandale, Ohio 45215

W. A. Compton
Solar Division International
Harvester
2200 Pacific Highway
San Diego, California

Dr. W. Cremens, Zone 402 1
Lockheed-Georgia
Department 72-14
Marietta, Georgia 30060

Dr. I. Crivelli-Visconti
Instituto Di Technologie
Universita Di Napoli
Napoli, Italia

Dr. D. Crachely
Rolls-Royce Ltd.
The Old Hall
Littleover, Derby, England

G. F. Davies
Clevite Corporation
7000 St. Clair Avenue, N.E.
Cleveland, Ohio 44110

L. W. Davis
Harvey Engineering Laboratories
Harvey Aluminum Company
19200 S. Western Avenue
Torrance, California 90509

Dr. L. M. Gillin
Aeronautical Research Laboratories
G.P.O. Box 4331
Melbourne, C. 1
Victoria, Australia

Dr. Rex B. Gosnell
Narmco Research/Development
Division
3540 Aero Court
San Diego, California 92123

G. C. Grimes
Southwest Research Institute
8500 Culebra Road
San Antonio, Texas 78206

K. R. Hanby
Battle Memorial Institute
505 King Avenue
Columbus, Ohio 43201

Prof. Tsuyoshi Hayashi
Structures Research Institute
University of Tokyo
Hongo 7-3-1, Bunkyo-Ku
Tokyo, Japan

Dr. M. Herman
Allison Division, GMC
P.O. Box 894
Indianapolis, Ind. 46206

H. Herring
NASA Langley Research Center
Structural Research Division
Langley Field, Virginia 23365

Edward J. Hughes
Aerospace Research Center
Singer General Precision
Little Falls, New Jersey 07424

Dr. R. C. Jones
Department of Civil Engineering
Massachusetts Institute of Technology
Cambridge, Massachusetts 02139

Dr. A. Kelly, Superintendent
Division Inorganic/Metallic Str.
National Physical Laboratory
Teddington, Middlesex, England

Major John Kershaw
MAMS
Wright Patterson AFB, Ohio 45304

N. Klimmek
Materials/Processes
North American Rockwell
Los Angeles Division
International Airport
Los Angeles, California 90045

Dr. R. H. Krock
P. R. Mallory Company
Northwest Industrial Park
Burlington, Massachusetts 01803

D. P. Laverty
Section Manager, Materials Tech.
Equipment Labs. Division of TRW
23555 Euclid Avenue
Cleveland, Ohio 44117

A. Lawley
Drexel Institute of Technology
Department of Metals Engineering
32 and Chestnut Streets
Philadelphia, Pennsylvania 19104

Dr. J. M. Lifshits
Department of Materials Engineering
Technion-Israel Inst. of Technology
Technion City, Haifa, Israel

Dr. E. M. Lende
AVCO Corporation
Lowell Industrial Park
Lowell, Massachusetts 01850

A. P. Levitt
Army Materials/Mechanics Research
Watertown, Massachusetts 02172

Librarian, Lycoming Division
AVCO Corporation
550 South Main Street
Stratford, Connecticut 06497

Dr. S. R. Lyon (MAMS)
AFML, Wright Patterson AFB
Ohio 45433

L. McCreight
General Electric Company
Valley Forge Space Tech.
P.O. Box 8555
Philadelphia, Pennsylvania 19101

G. D. Menke
Honeywell, Inc.
Minneapolis, Minnesota 55400

Dr. A. G. Metcalfe
Solar Division
International Harvester Company
2200 Pacific Highway
San Diego, California

Dr. Ishi Miura
Tokyo Medical Dental University
1-Chome,
Yushima Bunkyo-Ku
Tokyo, Japan

R. G. Moss
Jet Propulsion Laboratory
4800 Oak Grove Road
Pasedena, California 91103

Technical Librarian
Narmco Research/Development Div.
3540 Aero Ct.
San Diego, California 92123

M. C. Nicholas
Atomic Energy Research Establishment, Harwell
Berkshire, England

Technical Librarian
North American Rockwell
4300 E. 5th Avenue
Columbus, Ohio 43216

Dr. J. O Outwater
University of Vermont
Burlington, Vermont 05401

R. T. Pepper
Aerospace Corporation
Building Hl, MS 2281
P.O. Box 95085
Los Angeles, California 90045

R. K. Robinson
Ceramics/Composites Division
Battelle-Northwest
3000 Stevens Drive
Richland, Washington 99352

Dr. M. J. Salkind
United Aircraft Corporation
Sikorsky Aircraft Division
Stratford, Connecticut 06497

Dr. R. Sara
Union Carbide Company
Parma Technical Center
P.O. Box 6116
Cleveland, Ohio 44101

Prof. E. Scala
Bard Hall
Cornell University
Ithaca, New York 14850

Capt. W. A. Schulz
AFML
Wright-Patterson AFB
Ohio 45304

H. Shimizu
Marquardt Corporation
16555 Saticoy Street
Van Nuys, California 91409

Dr. D. M. Schuster
Sanida Corporation
Metallurgy Division 5431
P.O. Box 5800
Albuquerque, New Mexico 87115

Dr. I. J. Toth
TRW Equipment Laboratories
TRW Incorporated
23555 Euclid Avenue
Cleveland, Ohio 44117

A Toy
Material Sciences Department
TRW Systems Group
One Space Park
Redondo Beach, California 90278

B. A. Wilcox
Metal Science Group
Battelle Memorial Institute
505 King Street
Columbus, Ohio 43201

J. C. Withers
General Tech. Corp.
1821 Michael Faraday Drive
Reston, Virginia 22070

W. Wolkowitz
Grumman Aircraft Eng.
Bethpage, Long Island
New York 11714

Dr. G. Wirth
DFVLR
Institut fur Werkstoff-Forschung
505 Porz-Wahn
Linder-Hohe, Germany

Jack H. Ross (MANF)
Wright Patterson AFB
Ohio 45304

A. J. Yeast
Space Division
North American-Rockwell
12214 Lakewood Boulevard
Downey, California 90241